followed by mono Q chromatography (Pharmacia). $\alpha_{IIb}\beta_3$[17] was purified from human platelet by RGDSPK-Sepharose CL-4B. $\alpha_v\beta_3$- and $\alpha_{IIb}\beta_3$-binding assays were performed according to the modified method of Kouns et al.[18] EIA plates (Nunc) were coated with $\alpha_v\beta_3$ or $\alpha_{IIb}\beta_3$ and blocked with bovine serum albumin. In each reaction, the reaction mixture (20 mM Tris–HCl, 150 mM NaCl, 1 mM $CaCl_2$, and 1 mM $MgCl_2$, pH 7.4, 100 μl) including vitronectin (Calbiochem) or fibrinogen, added to the receptor-coated plate, was incubated for 4 h at 25 °C. Thereafter the ligand binding was measured using anti-vitronectin rabbit antibody (Calbiochem) and peroxidase-conjugated anti-rabbit IgG antibody (Capell) for $\alpha_v\beta_3$, or peroxidase-conjugated anti-fibrinogen antibody (Capell) for $\alpha_{IIb}\beta_3$, and 2,2′-azino-bis(3-ethylbenzthiazoline-6-sulfonic acid) (Sigma) as the substrate of peroxidase. The IC_{50} values were determined from measurement of absorbance at 415 nm.

6.11. Adhesion of human aorta smooth muscle cells to vitronectin

The adhesion of human aorta smooth muscle cells to vitronectin was measured as described before.[19] Briefly EIA plates (Nunc) were coated with human vitronectin (Calbiochem) and blocked with bovine serum albumin. The cell suspension of human aorta smooth muscle cells (50,000 cells/100 μl, Clonetics) in Dulbecco's modified Eagle's basal medium containing 0.1% bovine serum albumin was added to the vitronectin-coated plates and incubated for 1.5 h at 37 °C in the presence or absence of the test compounds. The adherent cells were stained with toluidine blue and calculated by measuring of absorbance at 405 nm after the cytolysis by SDS. The IC_{50} values were determined graphically from two or more independent experiments.

6.12. Platelet aggregation assay

Platelet aggregation was determined according to the previous method.[18] Human platelet-rich plasma obtained from healthy volunteers was prepared and the aggregation was induced with 5 μM ADP. The IC_{50} values were determined from two independent experiments.

Acknowledgments

We thank Miss Shigeko Miki and Mrs. Takako Miyara for mass spectral analysis.

References and notes

1. Hynes, R. O. *Cell* **1992**, *69*, 11.
2. Byzova, T. V.; Rabbani, R.; D'Souza, S. E.; Plow, E. F. *Thromb. Haemost.* **1998**, *80*, 726.
3. Fujishima, K.; Murakami, S.; Yamamoto, M.; Abe, M.; Ishikawa, M.; Ouchi, S.; Ajito, K. WO0154726, 2001.
4. Kubota, D.; Ishikawa, M.; Yamamoto, M.; Murakami, S.; Hachisu, M.; Katano, K.; Ajito, K. *Bioorg. Med. Chem.*, in press.
5. Brooks, P. C. *Drug News Perspect.* **1997**, *10*, 456, and references cited therein.
6. Dankwardt, S. M.; Smith, D. B.; Porco, J. A., Jr.; Nguyen, C. H. *Synlett* **1997**, 854.
7. Hochstein, F. A.; Els, H.; Celmer, W. D.; Shapiro, B. L.; Woodward, R. B. *J. Am. Chem. Soc.* **1960**, *82*, 3225.
8. Haubner, R.; Gratias, R.; Diefenbach, B.; Goodman, S. L.; Jonczyk, A.; Kessler, H. *J. Am. Chem. Soc.* **1996**, *118*, 7461.
9. Guari, Y.; van Es, D. S.; Reek, J. N. H.; Kamer, P. C. J.; van Leeuwen, P. W. N. M. *Tetrahedron Lett.* **1999**, *40*, 3789.
10. Talma, A. G.; Jouin, P.; De Vries, J. G.; Troostwijk, C. B.; Werumeus Buning, G. H.; Waninge, J. K.; Visscher, J.; Kellogg, R. M. *J. Am. Chem. Soc.* **1985**, *107*, 3981.
11. Reese, C. B.; Thompson, E. A. *J. Chem. Soc., Perkin Trans. 1* **1988**, 2881.
12. Ishikawa, M.; Kubota, D.; Yamamoto, M.; Kuroda, C.; Iguchi, M.; Koyanagi, A.; Murakami, S.; Ajito, K. *Bioorg. Med. Chem.*, in press.
13. Ishikawa, M.; Hiraiwa, Y.; Kubota, D.; Tsushima, M.; Watanabe, T.; Murakami, S.; Ouchi, S.; Ajito, K. *Bioorg. Med. Chem.*, in press.
14. (a) Keenan, R. M.; Miller, W. H.; Barton, L. S.; Bondinell, W. E.; Cousind, R. D.; Eppley, D. F.; Hwang, S. M.; Kwon, C.; Lago, M. A.; Nguyen, T. T.; Smith, B. R.; Uzinskas, I. N.; Yuan, C. C. K. *Bioorg. Med. Chem. Lett.* **1999**, *9*, 1801; (b) Pitts, W. J.; Wityak, J.; Smallheer, J. M.; Tobin, E.; Jetter, J. W.; Buynitsky, J. S.; Harlow, P. P.; Solomon, K. A.; Corjay, M. H.; Mousa, S. A.; Wexler, R. R.; Jadhav, P. K. *J. Med. Chem.* **2000**, *43*, 27.
15. Asanuma, H.; Kitakaze, M.; Node, K.; Sanada, S.; Ogita, H.; Takashima, S.; Asakura, M.; Minamino, T.; Tada, M.; Hori, M. *J. Am. Coll. Cardiol.* **2002**, *39*(Suppl 2), 300.
16. MeCN (200 ml) and EtOH (50 ml) were added to oleandomycin phosphate (25 g, 32 mmol) to prepare a solution. *p*-Toluenesulfonic acid (12 g, 65 mmol) was added to the solution, and the mixture was stirred at room temperature for 3.0 h. An aqueous Na_2CO_3 solution was added to the reaction solution, and the mixture was extracted three times with $CHCl_3$. The extract was dried over anhydrous Na_2SO_4 and was then concentrated under reduced pressure. The residue was purified by column chromatography on silica gel (ethyl acetate) to give ethyl α-L-oleandroside (3.75 g, 61%).
17. Pytela, R.; Pierschbacher, M. D.; Argraves, S.; Suzuki, S.; Rouslahti, E. *Methods Enzymol.* **1987**, *144*, 475.
18. Kouns, W. C.; Kirchhofer, D.; Hadvary, P.; Edenhofer, A.; Weller, T.; Pfenninger, G.; Baumgartner, H. R.; Jennings, L. K.; Steiner, B. *Blood* **1992**, *80*, 2539.
19. Liaw, L.; Almeida, M.; Hart, C. E.; Schwartz, S. M.; Giachelli, C. M. *Circ. Res.* **1994**, *74*, 214, and references cited therein.

The EMBO Journal (2006) 25, 3045–3055 | © 2006 European Molecular Biology Organization | All Rights Reserved 0261-4189/06
www.embojournal.org

THE EMBO JOURNAL

Glycosaminoglycan modification of neuropilin-1 modulates VEGFR2 signaling

Yasunori Shintani[1,4], Seiji Takashima[1,4,*], Yoshihiro Asano[1], Hisakazu Kato[1], Yulin Liao[1], Satoru Yamazaki[2], Osamu Tsukamoto[1], Osamu Seguchi[1,2], Hiroyuki Yamamoto[1,2], Tomi Fukushima[2], Kazuyuki Sugahara[3,5], Masafumi Kitakaze[2,*] and Masatsugu Hori[1]

[1]Department of Cardiovascular Medicine, Osaka University Graduate School of Medicine, Suita, Osaka, Japan, [2]Cardiovascular Division of Medicine, National Cardiovascular Center, Suita, Japan and [3]Department of Biochemistry, Kobe Pharmaceutical University, Higashinada-ku, Kobe, Japan

Neuropilin-1 (NRP1) is a co-receptor for vascular endothelial growth factor (VEGF) that enhances the angiogenic signals cooperatively with VEGFR2. VEGF signaling is essential for physiological and pathological angiogenesis through its effects on vascular endothelial cells (ECs) and smooth muscle cells (SMCs), but the mechanisms coordinating this response are not well understood. Here we show that a substantial fraction of NRP1 is proteoglycan modified with either heparan sulfate or chondroitin sulfate on a single conserved Ser. The composition of the NRP1 glycosaminoglycan (GAG) chains differs between ECs and SMCs. Glycosylation increased VEGF binding in both cell types, but the differential GAG composition of NRP1 mediates opposite responsiveness to VEGF in ECs and SMCs. Finally, NRP1 expression and its GAG modification post-transcriptionally regulate VEGFR2 protein expression. These findings indicate that GAG modification of NRP1 plays a critical role in modulating VEGF signaling, and may provide new insights into physiological and pathological angiogenesis.

The EMBO Journal (2006) **25**, 3045–3055. doi:10.1038/sj.emboj.7601188; Published online 8 June 2006
Subject Categories: signal transduction; proteins
Keywords: glycosaminoglycan; neuropilin-1; VEGF; VEGFR2

Introduction

Neuropilin-1 (NRP1) was originally discovered as a co-receptor for semaphorin-3A (Sema3A), an axon repellent factor (Kolodkin *et al*, 1997). However, NRP1 also acts as a co-receptor for vascular endothelial growth factor (VEGF), a molecule with no sequence or structural homology to Sema3A (Soker *et al*, 1998). VEGF (also referred as VEGF-A) is an essential factor promoting both embryonic angiogenesis and postnatal neovascularization. Additionally, VEGF plays a significant role in causing pathological angiogenesis associated with tumor growth, age-related macular degeneration, diabetic retinopathy, and other conditions (Ferrara *et al*, 2003). Indeed, a blocking anti-VEGF antibody that disrupts VEGF signaling is a promising anticancer therapy currently in development (Hurwitz *et al*, 2004).

VEGF has three receptors, VEGF receptor 1 and 2 (VEGFR1, VEGFR2), and neuropilin (Veikkola and Alitalo, 1999; Ferrara *et al*, 2003). VEGFR2 is the primary receptor mediating the angiogenic activity of VEGF (Shalaby *et al*, 1995; Ferrara *et al*, 2003), and NRP1 functions as a co-receptor to enhance VEGFR2 signaling (Soker *et al*, 1998). Indeed, genetic ablation of NRP1 leads to severely impaired vascular development (Kawasaki *et al*, 1999; Takashima *et al*, 2002; Gu *et al*, 2003), indicating that NRP1 is essential for VEGF-mediated angiogenesis.

In addition to promoting angiogenesis, VEGF is now thought to be required for the maintenance and stabilization of mature blood vessels (Zachary, 2001; Saint-Geniez and D'Amore, 2004). Signaling through VEGFR2, VEGF induces not only endothelial cell (EC) proliferation but also cell survival (Gerber *et al*, 1998), and the loss of VEGF signals in the choroidal endothelium is one factor promoting age-related macular degeneration (Blaauwgeers *et al*, 1999). Smooth muscle cells (SMCs), another important component of the vessel wall, also express both NRP1 (Kitsukawa *et al*, 1995; Kawasaki *et al*, 1999) and VEGFR2 (Grosskreutz *et al*, 1999; Ishida *et al*, 2001). However, SMCs in mature vessels typically do not respond to VEGF signals except in certain conditions such as atherosclerosis (Carmeliet, 2003; Jain, 2003; Khurana *et al*, 2004). Therefore, we wished to identify the mechanism(s) responsible for different cellular responses to VEGF in ECs and SMCs.

In this study, we demonstrate that a substantial fraction of NRP1 is proteoglycan modified with either heparan sulfate (HS) or chondroitin sulfate (CS) attached to a single conserved Ser. The type of NRP1 glycosaminoglycan (GAG) chain modification differs between ECs and SMCs. Finally, we show that the type of NRP1 GAG modification critically and differentially modulates VEGFR2 signals in SMCs and ECs.

Results

A substantial fraction of NRP1 is proteoglycan modified with HS or CS

The differential responsiveness of ECs and SMCs to VEGF could be explained by a number of factors, and we initially investigated the ability of VEGF to bind to these cells. When human coronary artery smooth muscle cells (CASMCs) were

*Corresponding authors. S Takashima, Department of Cardiovascular Medicine, Osaka University Graduate School of Medicine, 2-2 Yamadaoka, Suita, Osaka 565-0871, Japan. Tel.: +816 6879 3472; Fax: +816 6879 3473; E-mail: takasima@medone.med.osaka-u.ac.jp or M Kitakaze, Cardiovascular Division of Medicine, National Cardiovascular Center, Suita, Japan. E-mail: kitakaze@zf6.so-net.ne.jp
[4]These authors contributed equally to this work
[5]Present address: Laboratory of Proteoglycan Signaling and Therapeutics, Graduate School of Life Science, Hokkaido University, Frontier Research Center for Post-genomic Science and Technology, Sapporo, Japan

Received: 13 February 2006; accepted: 16 May 2006; published online: 8 June 2006

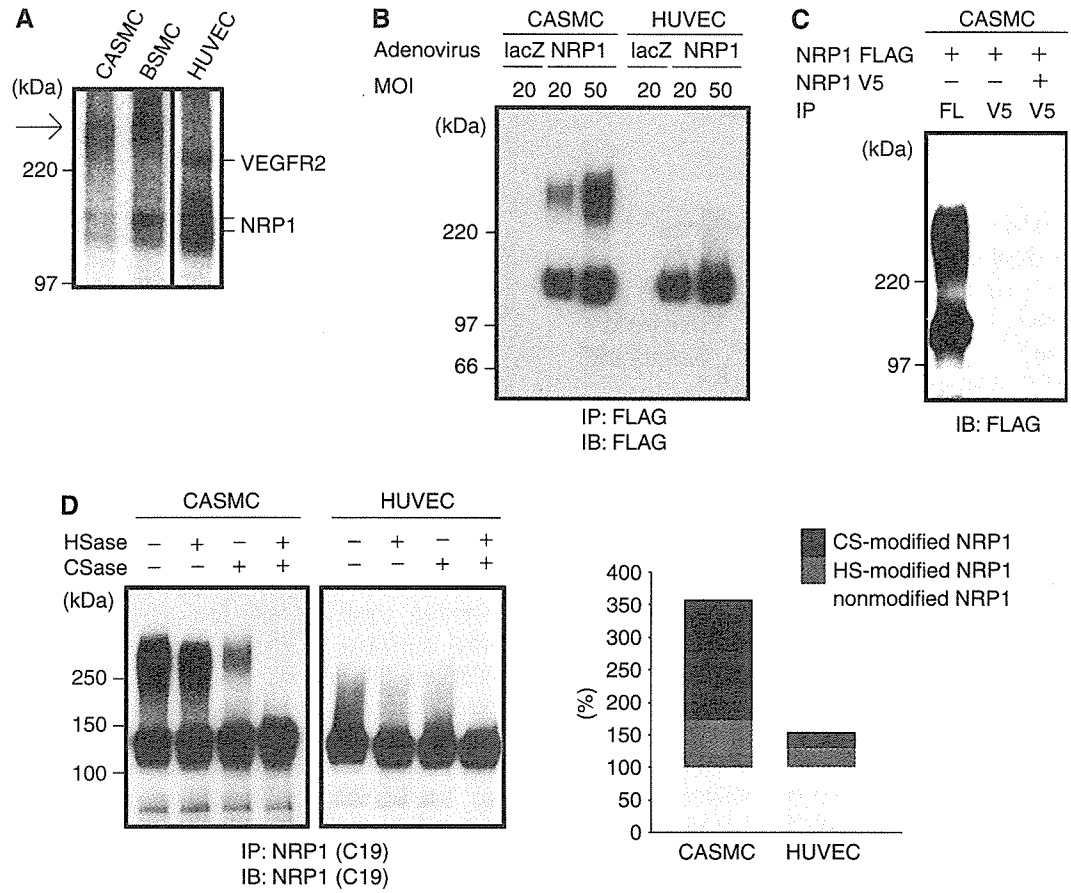

Figure 1 A substantial fraction of cellular NRP1 is proteoglycan, composed of either HS or CS. (**A**) ^{125}I-labeled VEGF is crosslinked to different proteins in ECs and SMCs. Arrow indicates VEGF-binding protein specifically seen in SMCs. CASMC: coronary artery smooth muscle cell; BSMC: bronchial smooth muscle cell; HUVEC: human umbilical vein endothelial cell. (**B**) Western blots of exogenously expressed NRP1 in either CASMCs or HUVECs. Adenovirus encoding FLAG-tagged NRP1 was transfected 2 days before analysis at the indicated MOI. LacZ-encoding adenovirus was used as a control. (**C**) The high molecular weight band was not simply a covalently linked homodimer of NRP1. Only FLAG-tagged NRP1 or both FLAG-tagged and V5-tagged NRP1 were transfected in CASMCs, and the cell lysates were immunoprecipitated and detected by the indicated antibody. (**D**) Endogenous NRP1 was modified by GAG chain addition in both SMCs and ECs. The upper band in CASMC immunoprecipitates disappeared following treatment with both HSase and CSase. HUVEC-expressed NRP1 is also GAG modified. The band intensity was analyzed and the proportion of each glycanated form of NRP1 was determined. Data are from three separate experiments. HSase: heparitinase; CSase: chondroitinase.

incubated with ^{125}I-labeled VEGF, we detected two distinct binding proteins after cell-surface crosslinking (Figure 1A). The lower band was also detected in human umbilical vein endothelial cells (HUVECs) and was identified as NRP1. However, the upper band was not found in HUVECs, and this band did not correspond to VEGFR2. In contrast, the upper band was also seen in bronchial smooth muscle cells (BSMCs) (Figure 1A), a non-vascular SMC, and, because NRP1 alone cannot transduce VEGF signals, we initially thought that this binding protein represented a new VEGF receptor. However, after transfection of CASMCs, but not HUVECs, with FLAG-tagged NRP1, we observed an identical upper molecular weight band when blotted with an anti-FLAG antibody (Figure 1B). The high molecular weight band was not simply a covalently linked homodimer of NRP1 (Figure 1C), and we reasoned NRP1 could undergo post-translational modification. Although NRP1 itself undergoes N-glycosylation, we found that the high molecular weight NRP1 was not a form of N-glycosylation or O-glycosylation by enzyme treatment and lectin blot (data not shown), but it did contain GAG chains. Indeed, treatment of NRP1 immunoprecipitates with both heparitinase and chondroitinase, which digest HS and CS, respectively, led to the disappearance of the upper band, whereas the lower band was not affected. Next, we investigated the composition of GAG-modified endogenous NRP1 in both CASMCs and HUVECs. Heparitinase slightly decreased the modified NRP1 band in CASMCs, whereas chondroitinase digested the majority of the GAG present on NRP1, indicating that CS was the dominant GAG modification of NRP1 (Figure 1D). In contrast, NRP1 in HUVECs was also modified, but to a much lesser extent than that seen in CASMCs, and HUVEC NRP1 contained almost equivalent amounts of CS and HS (Figure 1D). By analyzing the band intensity, we determined the degree of each modification relative to untreated samples (non-modified/HS-modified/CS-modified NRP1—CASMCs: 100%/79%/174%, HUVECs: 100%/27.3%/24.6%, respectively) (Figure 1D, right panel).

GAG chains are covalently added to Ser residues of the core protein contained within a Ser-Gly consensus sequence (Esko and Zhang, 1996). We mutated the nine consensus sequences present in NRP1, and the GAG chains are attached only to Ser^{612} (Figure 2A). As a single GAG chain cannot contain both HS and CS simultaneously, endogenous NRP1 exists as either

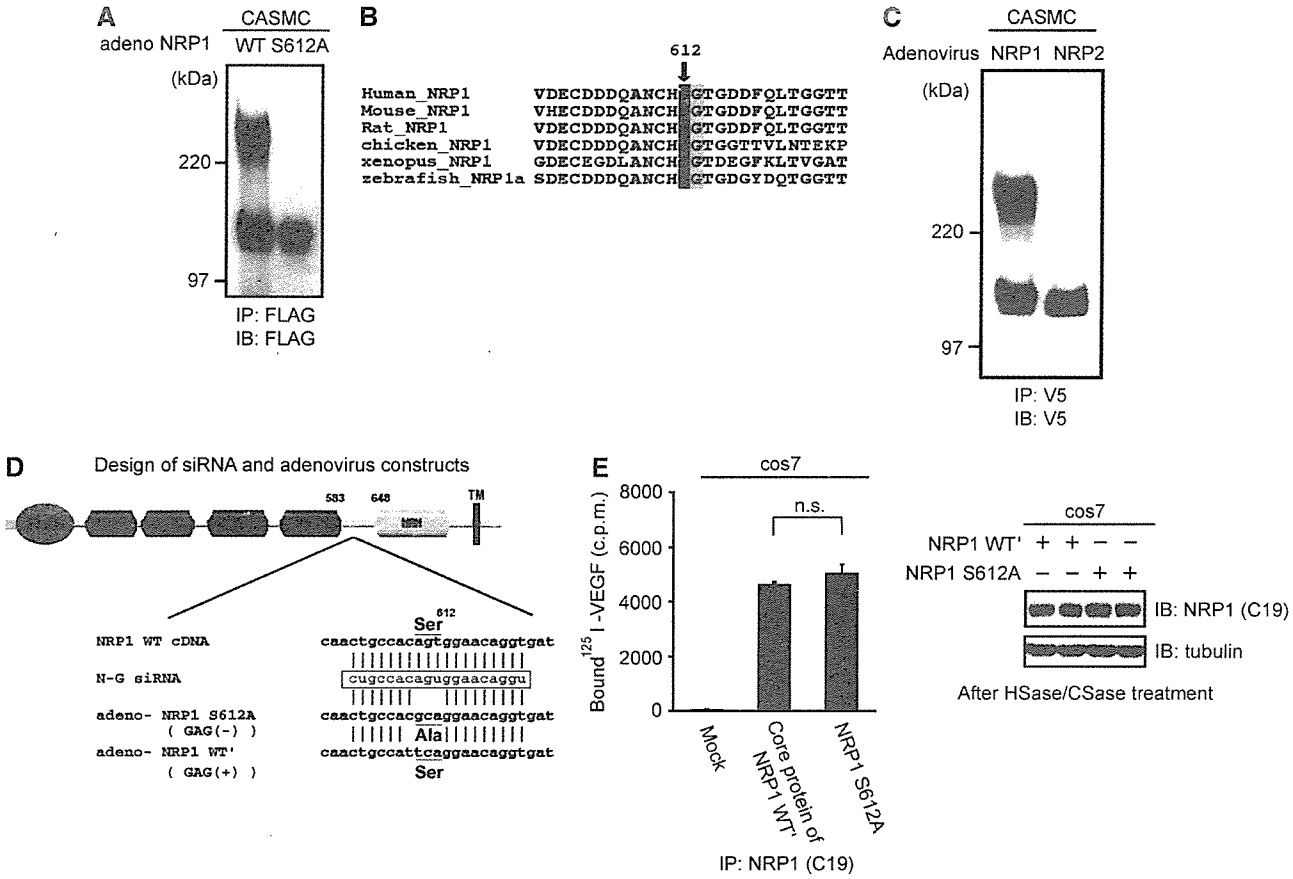

Figure 2 (**A**) NRP1 is GAG modified on a single Ser^{612} residue. CASMCs were transfected with adenoviral vectors encoding WT or S612A mutant NRP1. NRP1 S612A is not GAG modified. (**B**) Multiple alignments of NRP1 from different species. Ser^{612} is highly conserved among vertebrates. (**C**) NRP2, an NRP family member, is not GAG modified. (**D**) Design of siRNA and adenovirus constructs. Ser^{612} exists in the bridge region between the b1b2 and MAM domains. (**E**) Replacement of Ser^{612} by Ala^{612} of NRP1 did not change binding to VEGF. Cos7 cells were transfected with either NRP1 WT′ or S612A expression vector and preincubated with heparitinase (1.5 mU/ml), heparinase (1.5 mU/ml), and chondroitinase (20 mU/ml) in the culture medium at 37°C for 2 h to make NRP1 non-GAG form. After incubation with ^{125}I-labeled VEGF for 30 min at room temperature, cell lysates were immunoprecipitated by anti-NRP1 antibody, and the bound radioactivity was quantitated using a gamma counter. Data are from three independent experiments. For panel E, error bars represent s.e.

an HS proteoglycan or CS proteoglycan but not as a hybrid proteoglycan. Moreover, as shown in Figure 1D, non-modified NRP1 (130 kDa, the core protein) was always detected in both CASMCs and HUVECs. Ser^{612} is located in the bridge region between the b1b2 and MAM domains of NRP1 (Figure 2D), and multiple sequence alignments suggested that Ser^{612} was remarkably conserved among vertebrates (Figure 2B), and the peptide sequence around Ser^{612} was also well conserved, especially the acidic amino acids that are important for HS attachment (Esko and Zhang, 1996). NRP2, a mammalian homolog of NRP1, does not have this conserved Ser residue, and adenovirus-mediated expression of NRP2 in CASMCs demonstrated that NRP2 is not GAG modified (Figure 2C).

GAG modification of NRP1 enhances VEGF binding

Addition of both chondroitinase and heparitinase to culture medium completely digests all GAGs attached to other core proteins on the cell surface, and this would dramatically complicate the interpretation of any experiments using this technique. Therefore, to further investigate the function of the GAG of only NRP1, we used RNAi to knock down endogenous NRP1 while expressing mutant NRP1. We designed an siRNA, named N-G, targeting the GAG attachment site of NRP1 (Figure 2D). We further generated two NRP1-encoding adenovirus constructs: NRP1 S612A, in which Ser^{612} was replaced by Ala^{612} and there was a three-base mismatch with N-G siRNA; and NRP1 WT′, which contains the glycan accepting residue but had a four-base mismatch with N-G siRNA (Figure 2D). In cells transfected with N-G siRNA, transfection of both adenovirus constructs led to the expression of the appropriate NRP1 molecules. We confirmed that addition of FLAG tag to NRP1 does not affect VEGF binding (data not shown) and that the mutation itself (NRP1 S612A) did not change VEGF binding to the core protein of NRP1 (Figure 2E).

We next examined the ability of VEGF to bind to experimentally replaced NRP1 in both SMCs and ECs. Transfection of both N-G siRNA and equal multiplicity of infection (MOI) adenoviral constructs successfully replaced endogenous NRP1 with either the GAG-acceptor (NRP1 WT′) or mutated (NRP1 S612A) NRP1 (Figure 3A). Throughout these experiments, MOIs were used to generate NRP1 WT′ or S612A expression levels comparable to endogenous NRP1. To determine whether GAG modifications affect the ability of NRP1 to bind VEGF, we measured the binding of ^{125}I-labeled VEGF to FLAG-tagged NRP1 in these cells. After incubation with ^{125}I-labeled VEGF, cell lysates were immunoprecipitated with an

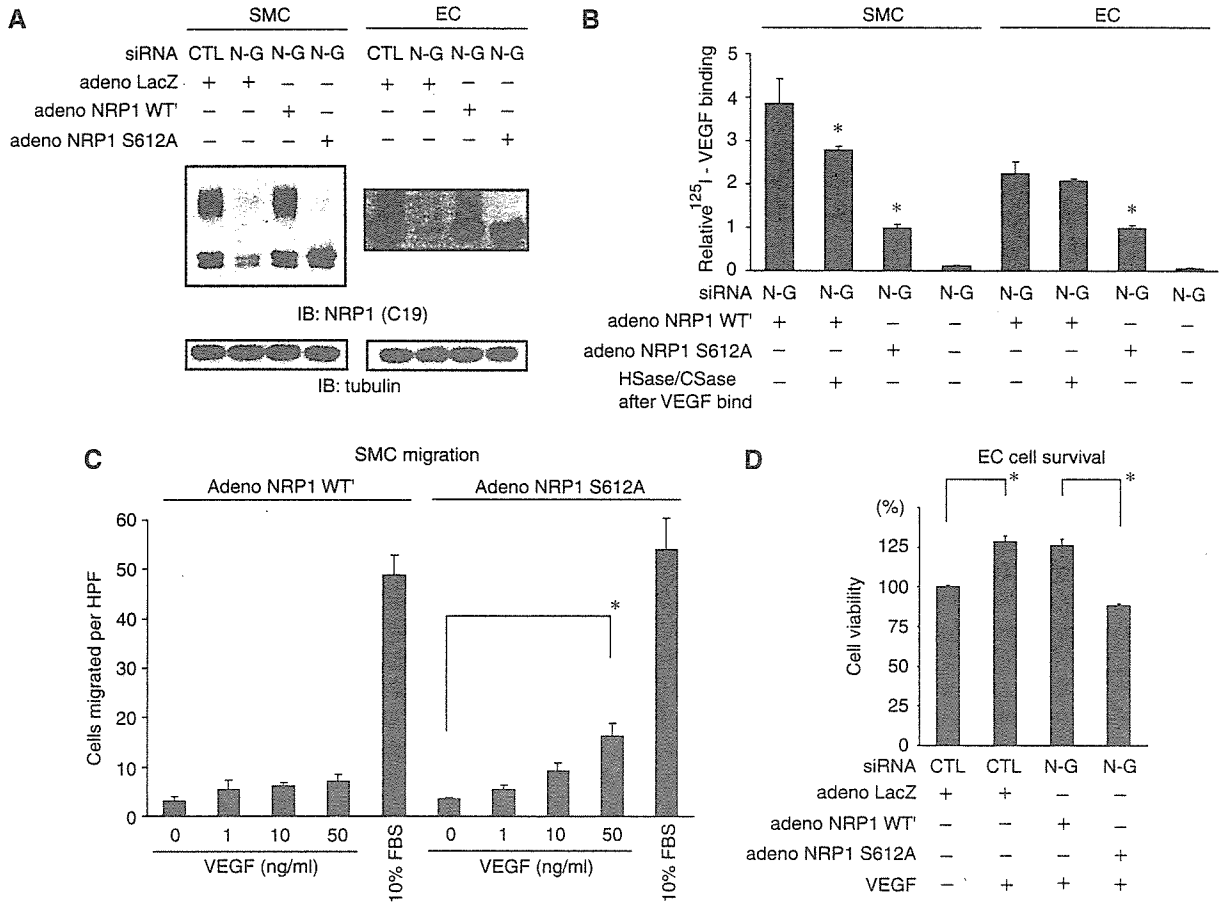

Figure 3 GAG modifications differentially affect NRP1 function in SMCs and ECs. (**A**) Experimental replacement of NRP1 in SMCs and ECs. After transfection with both N-G siRNA and adenoviral constructs, endogenous NRP1 was successfully replaced with either the glycanated form (NRP1 WT′) or non-glycanated form (NRP1 S612A) of NRP1. Tubulin was used as a loading control. (**B**) Addition of GAG to NRP1 enhances binding to VEGF in both types of cells. Two days after NRP1 replacement, cell lysates were immunoprecipitated with anti-FLAG antibody after incubation with ^{125}I-labeled VEGF (25 ng/ml) for 40 min at room temperature, and bound radioactivity was quantitated using a gamma counter. Heparitinase and chondroitinase treatment with these immunoprecipitates could not entirely eliminate the enhancement of VEGF binding. Data are from three independent experiments. (**C**) VEGF (50 ng/ml) induced greater cell migration in SMCs expressing non-modified NRP1 S612A than those expressing NRP1 WT′. Migrated cells were quantified by counting cells in three random high-power fields (HPF, × 200). Similar results were obtained from additional two independent experiments. (**D**) VEGF (50 ng/ml) increased cell viability in ECs expressing NRP1 WT′ to a greater extent than in ECs expressing NRP1 S612A. Data are from three independent experiments. For panels B–D, error bars represent s.e. $^*P<0.05$, versus adeno-NRP1 WT′ in panel B.

anti-FLAG antibody, and bound radioactivity was counted. NRP1 WT′ bound VEGF with 3.87- and 2.27-fold higher than NRP1 S612A in SMCs and ECs, respectively (Figure 3B). We found that heparitinase and chondroitinase treatment with these immunoprecipitates could not entirely eliminate the enhancement of VEGF binding (Figure 3B), different from the results of Figure 2E in which we showed that VEGF equally binds NRP1 WT′ and S612A pretreated with heparitinase and chondroitinase before the exposure to VEGF. These results suggest that GAG modifications of NRP1 in SMCs and ECs enhance VEGF binding mainly to NRP1 core protein and not to only GAG chain of NRP1.

NRP1 GAG modifications lead to differential VEGF responsiveness in SMCs and ECs

We next investigated whether GAG modifications of NRP1 in both SMCs and ECs affected cellular responsiveness to VEGF. VEGF increases the motility of vascular SMCs (Grosskreutz *et al*, 1999; Ishida *et al*, 2001), and induces proliferation, migration, and cell survival in ECs (Ferrara *et al*, 2003). These actions are primarily mediated through the VEGFR2 signaling pathway likely in conjunction with NRP1.

Notably, VEGF induced the migration of SMCs expressing NRP1 S612A (non-modified) stronger than those expressing NRP1 WT′ (GAG modified) (Figure 3C). In contrast, VEGF increased the viability of ECs expressing NRP1 WT′ to a greater extent than those expressing NRP1 S612A (Figure 3D). The observed increased viability seen in ECs expressing NRP1 WT′ in response to VEGF is consistent with the increased VEGF binding shown in Figure 3B. However, the decreased motility seen in SMCs expressing NRP1 WT′ was unexpected. To further explore this discrepancy, we examined the influence of different GAG chains on the expression of VEGR2 and the formation of the VEGF–VEGFR2–NRP1 ternary complex, both important determinants of VEGF signaling (Soker *et al*, 2002).

We first analyzed VEGFR2 protein expression in cells expressing either NRP1 WT′ or S612A. In SMCs expressing S612A mutant, VEGFR2 expression was two-fold higher than in cells expressing NRP1 WT′ (Figure 4A (left) and B), but

expression of either NRP1 WT′ or S612A did not affect VEGFR2 expression in ECs (Figure 4A (right) and B). The increased VEGFR2 protein expression in SMCs was not accompanied by changes in mRNA levels (Figure 4C), indicating that post-transcriptional mechanisms regulate VEGFR2 expression.

Both the extent of GAG modification and the predominant GAG chain added (i.e. HS or CS) differ between ECs and SMCs. Therefore, we examined whether the type of GAG modification affected ternary complex formation. We used enzymatic digestions and ^{125}I-labeled VEGF binding to assess the contribution of CS- and HS-modified NRP1 to VEGF binding, and found that all forms of NRP1 bound VEGF equally well (Figure 4D). We next examined the ability of GAG-modified NRP1 to associate with VEGFR2 in the presence of VEGF by co-immunoprecipitation. After pretreatment with heparitinase and/or chondroitinase, V5-tagged VEGFR2 was precipitated from SMC lysates in the presence of VEGF. As shown in Figure 4E, CS-modified NRP1 minimally associated with VEGFR2 compared to non-modified or HS-modified NRP1.

Thus, in SMCs, GAG-modified NRP1 post-transcriptionally downregulates VEGFR2 expression, and CS-modified NRP1 may act as a decoy receptor, rather than a co-receptor. It is likely that a combination of these factors explains the differences in VEGF activity seen in SMCs expressing NRP1 WT′ or S612A (Figure 3C).

Based on the results of receptor complex formation in the presence of VEGF in Figure 4E, we hypothesized that NRP1 might affect VEGFR2 internalization/degradation after ligand binding, because degradation of the receptor tyrosine kinase is an important regulator of signaling intensity (Duval *et al*, 2003; Rubin *et al*, 2005). Before exposure to VEGF, VEGFR2 expression was not different between ECs expressing NRP1 WT′ and S612A (Figure 4A). However, the rate of VEGFR2 degradation was decreased in NRP1 WT′ ECs compared to NRP1 S612A ECs. Phosphorylated VEGFR2 was also much higher in ECs expressing NRP1 WT′ than those expressing NRP1 S612A at any time points after VEGF (Figure 4F). These results suggested that the GAG modification of NRP1 enhances VEGF signaling in ECs by delaying the degradation of VEGFR2 in the presence of VEGF, and not just by the enhancement of VEGF binding.

NRP1 post-transcriptionally modulates VEGFR2 expression

NRP1 knockout mice exhibit severely impaired vascular development and die around E13.5 (Kitsukawa *et al*, 1995; Kawasaki *et al*, 1999). VEGF has several splicing isoforms (its major forms in mice are $VEGF_{120, 164, 188}$) and NRP1 does not bind $VEGF_{120}$. In contrast, VEGFR2 can bind all of VEGF isoforms. Although NRP1 is a common receptor for both VEGF and Sema3A, impaired VEGF signaling is responsible for the observed vascular defects in these mice (Gu *et al*, 2003). However, the vascular defect in NRP1−/− mice is more severe than that seen in $VEGF^{120/120}$ mice, in which only $VEGF_{120}$ is expressed (Carmeliet *et al*, 1999; Stalmans *et al*, 2003). Thus, NRP1 appears to play a more prominent role in VEGF signaling than simply functioning as a co-receptor for some VEGF isoforms. Based on the results that CS-dominant GAG of NRP1 negatively affects VEGFR2 expression levels in SMCs, we hypothesized that NRP1 basically stabilizes VEGFR2 leading to increased expression. Thus, VEGFR2 expression should be lower in NRP1−/− mice, leading to a more pronounced vascular phenotype.

To test this hypothesis in cells, we knocked down NRP1 in ECs using siRNA. Before the addition of VEGF, VEGFR2 expression was substantially decreased in cells transfected with NRP1 siRNAs (Figure 5A). Two siRNAs targeting NRP1 were used to exclude the possibility of an off-target effect of RNAi. VEGFR2 mRNA levels were unaffected by NRP1 knockdown, however (Figure 5B). Additionally, VEGFR1, another VEGF receptor, was not affected by either NRP1 siRNA, suggesting that NRP1 specifically regulates VEGFR2 expression (Figure 5A). As VEGFR2 protein level was not associated with transcription level, we conducted pulse-chase experiments in HUVECs treated with NRP1 siRNA to determine the rate of VEGFR2 degradation in the absence of VEGF. Notably, we found that the rate of VEGFR2 degradation was not changed by NRP1 knockdown (Figure 5C), which was different from the results in the presence of VEGF (Figure 4F).

We next examined whether the ability of NRP1 to promote VEGFR2 expression was specific for ECs, and we generated Flp293/VEGFR2 cells stably expressing VEGFR2. These cells express much less NRP1 than either ECs or SMCs. When these cells were transfected with NRP1, NRP1 was GAG modified similar to ECs (Figure 5D), and VEGFR2 expression was substantially upregulated (Figure 5D). VEGFR2 transcription was not altered by NRP1 expression (data not shown). Finally, when transfected cells were examined by confocal microscopy, NRP1-expressing cells had substantially higher cell-surface VEGFR2 levels compared to non-transfected adjacent cells (Figure 5E).

Discussion

NRP1 GAG modifications differentially regulate VEGF responsiveness in SMCs and ECs

In this study, we showed that a substantial fraction of NRP1 is proteoglycan modified with either HS or CS on a single conserved Ser residue. Additionally, both the degree and length of GAG modification and the predominant side chain added differ between ECs and SMCs. In both ECs and SMCs, GAG modifications enhanced VEGF binding, but GAG addition to NRP1 in ECs enhanced VEGF–VEGFR2 signaling. In contrast, GAG-modified NRP1 negatively affected VEGF activity in SMCs. Interestingly, in SMCs, GAG modification of NRP1 post-transcriptionally downregulates VEGFR2 expression, and CS-modified NRP1, the major form of NRP1 in SMCs (about 50% of total NRP1), may act as a decoy receptor, rather than a co-receptor.

The mechanism by which the addition of GAGs to NRP1 enhanced VEGF signals in ECs remains unclear. We speculate that the addition of HS chains to NRP1 promotes multimerization. Exogenous heparin and HS bind NRP1 via its b1b2 domain and increase VEGF binding to NRP1 and VEGFR2 (Gitay-Goren *et al*, 1992; Mamluk *et al*, 2002). Additionally, heparin can induce NRP1 multimerization in the presence or absence of ligands (Fuh *et al*, 2000; Mamluk *et al*, 2002). Binding between the NRP1 b1b2 domain and HS requires only eight highly sulfated monosaccharide units (Mamluk *et al*, 2002). Generally, in a single HS chain, sulfated sugar residues occur in multiple clusters (containing 6–10 sugars)

separated by regions of low sulfation (Gallagher, 2001). We estimated the length of a single HS chain of NRP1 as about 50 kDa in ECs including at least 200 monosaccharide units, and this modification is sufficient to bind multiple NRP1 molecules. Therefore, we speculate that a single NRP1 HS chain could bind multiple NRP1 molecules and promote NRP1 clustering. Such an NRP1 cluster could recruit substantial amounts of VEGFR2, and, in the presence of VEGF, increase the binding frequency without affecting the dissociation constant. When the receptor complex with VEGF and VEGFR2 is formed, VEGFR2 might stabilize and escape internalization/degradation, and as a result it enhances VEGF signal (as in Figure 4F). In contrast to HS, the role of CS in VEGF signaling has not been well investigated. We found that only chondroitin sulfate-E (CS-E, a subclass of CS chains) enhances VEGF binding to NRP1 in ECs like heparin

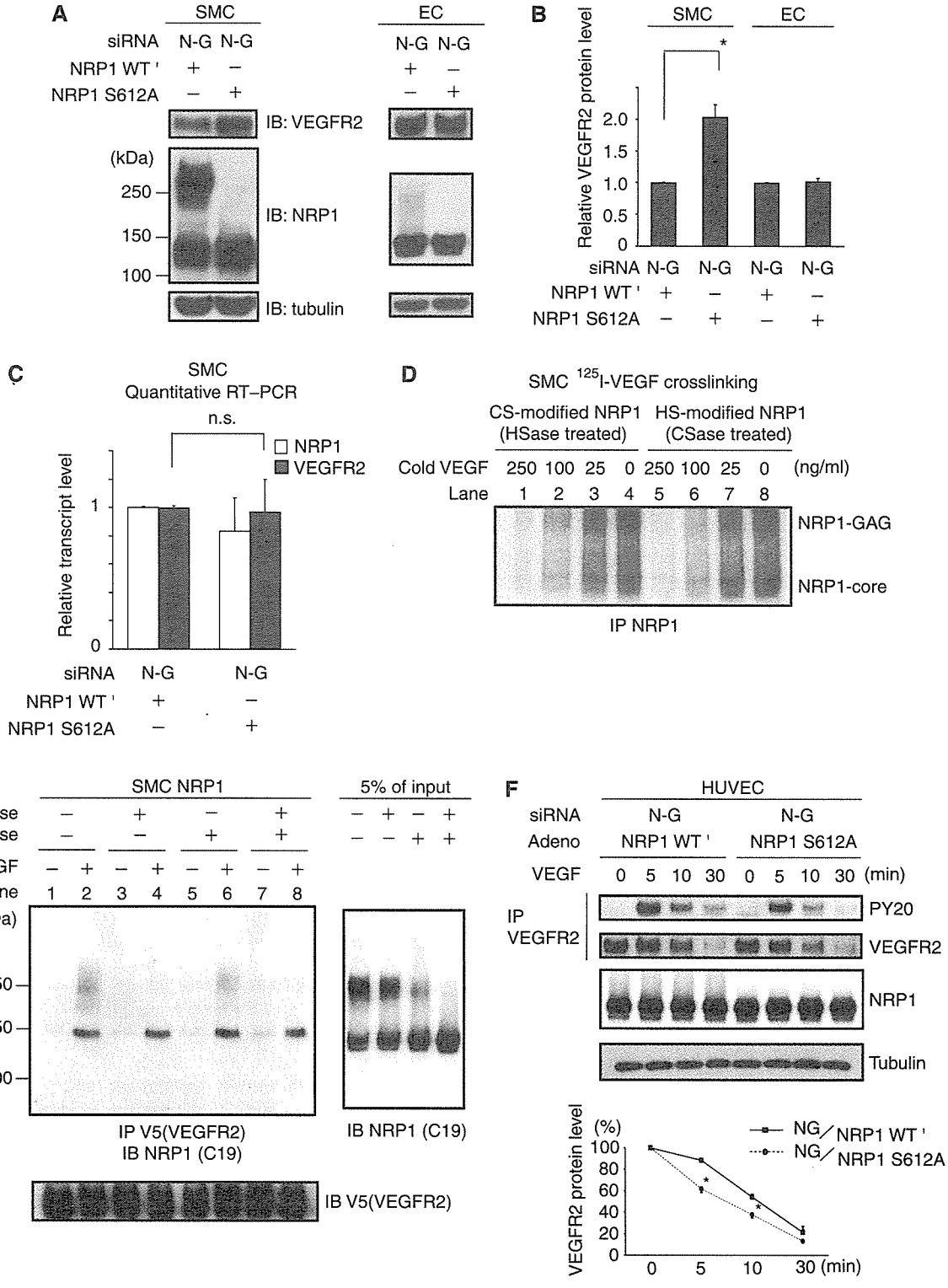

(Supplementary data A). However, CS-E is a very rare modification, and we found no CS-E on the GAG chains of NRP1 in both SMCs and ECs in our preliminary analysis (data not shown). Furthermore, chondroitinase treatment with immunoprecipitated NRP1 after VEGF did not change the VEGF binding to NRP1 in both ECs and SMCs, whereas heparitinase treatment decreased (Supplementary data B). These results suggested that endogenous CS, which usually does not contain CS-E, has no beneficial or unprofitable effect on VEGF binding to NRP1 core and it is unlikely that endogenous CS on the cell surface including CS chains of NRP1 could induce NRP1 multimerization.

We have not ruled out the possibility that GAG modification of NRP1 induces conformational changes in the binding surface between VEGF and NRP1, or between VEGFR2 and NRP1, and the addition of CS to NRP1 might hamper such

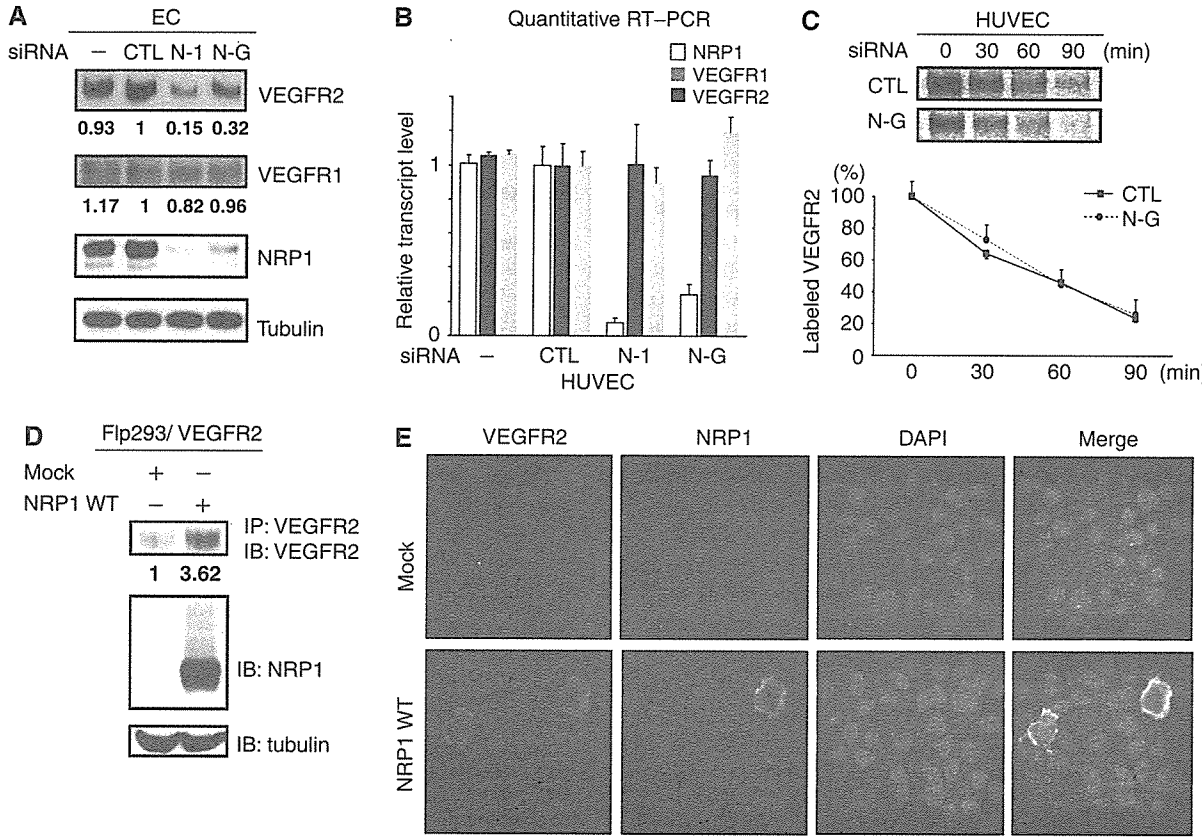

Figure 5 NRP1 post-transcriptionally regulates the expression of VEGFR2. (**A**) Both NRP1 siRNAs (N-G, N-1) decreased VEGFR2 expression. In contrast, VEGFR1 was not influenced by NRP1 knockdown. Tubulin was used as a loading control. Data are representative of at least three independent experiments. (**B**) Transcription levels of both VEGFR1 and VEGFR2 were not influenced by NRP1 knockdown. Each sample was analyzed in duplicate and experiments were performed in triplicate for the full set of genes. (**C**) Pulse–chase experiments in HUVECs. The rate of degradation of VEGFR2 was not changed by NRP1 knockdown. Data are from four independent experiments. (**D**) NRP1 significantly upregulated VEGFR2 protein levels in Flp293/VEGFR2 cells. Transfected NRP1 in Flp293/VEGFR2 cells was GAG modified similar to ECs. Data are representative of two independent experiments. (**E**) NRP1 regulates cell-surface VEGFR2 expression. Transient expression of FLAG-tagged NRP1 WT upregulated the cell membrane-associated VEGFR2 expression compared to adjacent non-transfected cells. Flp293/VEGFR2 cells were transfected with either NRP1 WT or mock and stained without permeabilization using anti-VEGFR2 (green) and anti-FLAG-Cy3 (red). Blue: DAPI nuclear staining. For panels A and C, numeric represents the mean of band intensity of three experiments. For panel B, error bars represent s.e.

Figure 4 Different roles of the GAG of NRP1 on VEGFR2 in SMCs. (**A**) Experimental replacement with NRP1 S612A increased VEGFR2 expression in SMCs, but replacement did not affect VEGFR2 expression in ECs. Two days after transfection with siRNA and adeno-NRP1, cells were analyzed by Western blotting. Data are representative of at least three independent experiments. (**B**) Quantitative results of Western blot. (**C**) Experimental replacement with NRP1 S612A increased VEGFR2 protein expression without any transcriptional change in SMCs. Each sample was analyzed in duplicate and the experiments were performed in triplicate for the full set of genes. (**D**) CS-modified NRP1 had the same affinity for VEGF as HS-modified NRP1 and non-modified NRP1. Note that ^{125}I-labeled VEGF bound CS-modified NRP1 with a similar ratio before crosslink (upper band in lanes 4 and 8, CS-modified NRP1:HS-modified NRP1 = 2:1). Increasing amounts of cold VEGF equally inhibited ^{125}I-labeled VEGF binding to all forms of NRP1. (**E**) Co-immunoprecipitation of NRP1 with VEGFR2. CS-modified NRP1 (left panel, about 250 kDa in lane 4) minimally associated with VEGFR2 compared to non-modified (130 kDa, in lanes 2, 4, 6, 8) and HS-modified NRP1 (about 250 kDa in lane 6), although there was a two-fold excess of CS-modified NRP1 compared to HS-modified NRP1 at input (right panel). The membrane was stripped and re-probed with anti-V5 as a loading control. Data are representative of at least three independent experiments. (**F**) The rate of VEGFR2 degradation was decreased in NRP1 WT′ ECs compared to NRP1 S612A ECs. Phosphorylated VEGFR2 was also much higher in NRP1 WT′ ECs than in NRP1 S612A ECs at any time point after VEGF. Data are representative of at least three independent experiments. For panels B, C, F, error bars represent s.e. *$P<0.05$, versus NG/ NRP1 S612A at the same period as in panel F. HSase: heparitinase; CSase: chondroitinase.

allosteric effects in SMCs. Further structural studies examining the interaction of GAG-modified NRP1 with VEGFR2 will clarify this issue.

NRP1 is also a receptor for Sema3A (Kolodkin *et al*, 1997). It was recently found that GAG regulates the function of Sema5A, a member of a different class of the semaphorin family. Sema5A is able to exert both attractive and repulsive effects, depending on association with HS and CS, respectively (Kantor *et al*, 2004). This intriguing report raises the possibility that GAG chains of NRP1 might also regulate Sema3A binding and function. Further study is needed to clarify the role of GAG modifications on NRP1/Sema3A signaling. Furthermore, it was recently reported that FGF2 binds NRP1 (West *et al*, 2005). It might be interesting to search the role of GAG modifications of NRP1 on FGF2 signaling.

What is the physiological relevance of GAG-mediated differences in VEGF responsiveness in vascular cells?

The addition of GAG chains to NRP1 led to opposite effects on VEGFR2 signaling in ECs and SMCs. SMCs migrate in response to VEGF, and this migration is mediated mainly through VEGFR2. However, cell density or passage number affects SMC response to VEGF (Ishida *et al*, 2001). We identified a specific lot of SMCs expressing comparable levels of VEGFR2 as ECs. In these cells, the pattern of NRP1 GAG modification was similar to that of ECs seen in this study (Y Shintani and S Takashima, unpublished observations). Additionally, GAG chain modifications changed with time in culture or by incubating in ischemic conditions (preliminary data). Thus, different ill-defined culture conditions can cause changes in GAG addition to NRP1, and this can affect VEGF signaling in both SMCs and ECs.

Based on the present results, it appears that differential GAG chain addition to NRP1 can mediate opposite responses to VEGF in ECs and SMCs in mature blood vessels. In contrast, during active angiogenesis, SMCs need to migrate and enclose ECs to form complete vessels. Under these circumstances, both ECs and SMCs might express NRP1 with short GAG chains and respond similarly to VEGF for efficient vessel formation. Indeed, VEGF has also been recently implicated in the normal development of SMC-surrounded coronary arteries and pericyte coverage in the retinal vasculature (Benjamin *et al*, 1998; Carmeliet *et al*, 1999). Further investigation will be needed to clarify the *in vivo* composition of GAG chains of NRP1.

NRP1 post-transcriptionally regulates the expression of VEGFR2

We demonstrated that knockdown of NRP1 by RNAi post-transcriptionally reduced VEGFR2 expression in ECs, suggesting that NRP1 positively regulates the expression of VEGFR2. In contrast, GAG addition to NRP1 in SMCs eliminated this effect. As the transcription of VEGFR2 was not affected by NRP1 expression or GAG modification, we conclude that VEGFR2 expression is post-transcriptionally regulated by NRP1.

Cell-surface proteins undergo a complex process including co-translational folding, post-translational modifications, and transport through various cellular compartments including the ER and Golgi apparatus. Recent reports suggest that stable cell-surface receptor expression in the absence of ligand sometimes requires a specific adaptor protein or co-receptor (McLatchie *et al*, 1998; Loconto *et al*, 2003; Saito *et al*, 2004). Most identified receptors are complex proteins with seven transmembrane domains, but a type I membrane receptor such as VEGFR2 could also require such an adaptor or co-receptor, for example, NRP1. NRP1 and VEGFR2 might interact in the absence of VEGF and the addition of CS to NRP1 interferes with the trafficking and/or stability of VEGFR2.

Our findings suggested that NRP1 is a key modulator of VEGF signaling. Further studies and technical advances are needed to precisely characterize the importance of particular GAG modifications on VEGF signaling *in vitro* and *in vivo*. However, the role of NRP1 and its post-translational modifications may provide new insights into the growth of vascular networks in physiological and pathological conditions.

Materials and methods

Materials

We utilized the following commercially available antibodies: anti-NRP1 antibody (C-19, Santa Cruz Inc.), anti-human VEGFR2 for Western blot (A-3, Santa Cruz Inc.), for immunofluorescent study (ab9530, Abcam), for immunoprecipitation (C-1158, Santa Cruz Inc.), anti-alpha-tubulin (clone B-5-1-2, Sigma), anti-VEGFR1 (C-17, Santa Cruz Inc.), anti-FLAG M2 (Sigma), anti-V5 (Invitrogen), PY20-HRP-conjugated antibody (BD Biosciences). Heparitinase, heparinase, and chondroitinase were purchased from Seikagaku Corp.

Preparation, radioiodination of VEGF, and chemical crosslinking

Recombinant human $VEGF_{165}$ was prepared in Hi5 cells using the baculovirus system (Invitrogen) and purified with two-step chromatography to over 95% purity as determined by silver stain. $Na^{125}I$ was purchased from Amersham Biosciences, and ^{125}I-labeled VEGF was prepared using IODO-BEADS (Pierce). ^{125}I-labeled VEGF crosslinking study was performed as described previously (Soker *et al*, 1998). Briefly, cells were grown to 90–95% confluence in a 60 mm collagen 1-coated dish and labeled with ^{125}I-labeled VEGF (25 ng/ml) using DSS (Pierce) according to the manufacturer's instructions. Cells were lysed with 1% Nonidet P-40 containing buffer (1% Nonidet P-40, 0.15 M NaCl, 20 mM Tris pH 7.2, including protease inhibitor cocktail (Nacalai)) and then subjected to SDS–PAGE using 5–10% gradient gel (Bio-Rad). Bound ^{125}I-labeled VEGF was detected by autoradiography using the BAS system (Fuji). For competitive binding analysis (Figure 4D), CASMC was transfected with FLAG-tagged NRP1 at MOI 10 2 days before the experiment. After crosslinking, cells lysates were immunoprecipitated with anti-FLAG M2 antibody, and immunoprecipitates were then subjected to heparitinase (1.25 mU/ml) or chondroitinase (250 mU/ml) treatment. Cold VEGF was added 5 min before ^{125}I-labeled VEGF for assessing binding affinity.

Expression vector and adenovirus constructs

Human NRP1 cDNA was obtained as described previously (Soker *et al*, 1998). In this experiment, all construction was performed using the Gateway system (Invitrogen) according to the manufacturer's instructions. With PCR primer designed to include or delete stop codon of NRP1, the amplified fragment was inserted into pENTR/D-TOPO (Invitrogen), named pENTR/NRP1 or pENTR/NRP1-cV5, respectively. To generate N-terminal FLAG-tagged NRP1 (NRP1 FLAG), FLAG epitope (DYKDDDDK) was inserted just after the signal sequence of NRP1 (between Lys^{26} and Cys^{27}) by PCR-based mutagenesis using pENTR/NRP1 as a template. Both NRP1 WT' and S612A were also generated by PCR-based mutagenesis (primer design is shown in Figure 2C). All the NRP1 constructs were recombined to mammalian expression vector, pEF-DEST51 (Invitrogen) and pAd/CMV/V5-DEST (Invitrogen). Adenovirus constructs were generated using ViraPower Adenoviral Expression System (Invitrogen) essentially as described by the manufacturer. Recombined vectors along with the supplied pAd/CMV/V5-DEST/lacZ were transfected into host HEK293A cells (Invitrogen). NRP2

and VEGFR2 cDNAs were cloned into pENTR/D-TOPO from HUVEC cDNA. Both adenoviruses and expression vectors of non-tagged and V5-tagged NRP2 and VEGFR2 were generated as those of NRP1.

Cell culture

HUVECs, human CASMCs, human BSMCs, and human aortic smooth muscle cells (AoSMCs) were obtained from Clonetics. They were cultured in endothelial and smooth muscle cell medium (Clonetics) and used up to passage 5.

Treatment with heparitinase and chondroitinase, and analysis of the proportion of each glycanated NRP1

Cells were lysed with lysis buffer (0.15 M NaCl, 1 mM EDTA, 20 mM Tris pH 7.2, including protease inhibitor cocktail (Nacalai)). The aliquots of lysates were incubated with anti-NRP1 antibody (C-19), followed by addition of Protein G Sepharose (Amersham Bioscience) for 1–2 h at 4°C. Bound NRP1 was then subjected to heparitinase and/or chondroitinase treatment in enzyme-contained buffer (1% Nonidet P-40, 0.15 M NaCl, 5×10^{-5} M Ca^{2+}, 20 mM Tris pH 7.2, including heparitinase (1.25 mU/ml) and/or chondroitinase (25 mU/ml)) at 37°C for 1 h. Enzyme-treated immunoprecipitates were subjected to SDS–PAGE and Western blotting. By analyzing the band intensity using ImageJ software (version 1.34s), the proportion of each glycanated form of NRP1 was determined.

RNAi and adenovirus transfection, experimental replacement of NRP1 with/without GAG

HUVECs at 50–70% confluency were transfected with the indicated siRNA duplexes using Optifect (Invitrogen) according to the manufacturer's instructions. AoSMCs (for Western blot, RT-PCR, VEGF binding and migration assay) or CASMCs (for ^{125}I-labeled VEGF crosslinking and co-immunoprecipitation) at 80–90% confluency were transfected with Lipofectamine 2000 (Invitrogen). SiRNA was transfected at 50 nM in a 60 or 100 mm dish 4–6 h after plating. After another 4 h, adeno- LacZ, NRP1 WT′, or S612A was infected at an MOI of 2 (for ECs) or 4–6 (for SMCs). NRP1 siRNAs were synthesized by Dharmacon Inc., and siRNAs sequences were as follows: N-G: sense 5′-cugccacaguggaacaggu-dTdT, N-1: sense 5′-gagagguccugaauguucc-dTdT. N-1 was the same sequence that had been previously reported (Bachelder *et al*, 2003). SiRNA for non-silencing control used in this study was targeted for GL2: sense 5′-cguacgcggaauacuucga-dTdT (Elbashir *et al*, 2001). We chose this oligonucleotide as control because VEGFR2 and NRP1 expression level was not affected as compared with non-transfected cells, different from other several non-silencing control siRNAs that are commercially available.

^{125}I-labeled VEGF binding to NRP1

Two days after transfection with siRNA (N-G) and adeno-NRP1 WT′ or S612A, both SMCs and ECs were incubated with ^{125}I-labeled VEGF (25 ng/ml) for 40 min at room temperature. The cells were washed twice with PBS and lysed with lysis buffer (0.15 M NaCl, 1 mM EDTA, 20 mM Tris pH 7.2, including protease inhibitor cocktail (Nacalai)). Cell lysates were immunoprecipitated with anti-FLAG M2 agarose (Sigma) for 1 h at 4°C. After washing with buffer twice, the immunoprecipitates were subjected to gamma counter (Beckman).

Cell migration assay

Effects of VEGF on SMCs migration were studied using 24-well Transwell® microplate (Corning Inc.). Pore (8.0 μm) polystyrene filters were treated with 10 μg/ml fibronectin (Sigma). Two days after the transfection with RNAi (N-G) and respective adenovirus (NRP1 WT′ or S612A), AoSMCs were trypsinized and then loaded into the inner chamber at 1×10^4 cells/well. After incubation with or without VEGF (1, 10, 50 ng/ml) or 10% FBS at 37°C for 6 h in a CO_2 incubator, the upper side of the filters containing non-migrated cells was wiped and rinsed. The filters were fixed and stained with Diff-Quik®. Migrating cells were quantified by counting cells in each well at three random high-power fields (×200). All groups were studied in triplicate.

Cell viability

Cell viability was assessed with a CellTiter 96 Aqueous One Solution Cell Proliferation Assay System (Promega). HUVECs were plated in a 96-well culture plate at a density of 5×10^4 cells/well in 0.5% FBS in EBM2 medium (Clontech). Six hours after plating, siRNA was transfected using Optifect at 100 nM; consequently, adenovirus addition was performed at MOI 2. Serum starvation with or without VEGF (50 ng/ml) was performed 24 h after transfection and MTS reagent was added to each well 24 h later, and optical absorbance at 490 nm was measured with a microplate reader.

Quantitative RT–PCR

Total RNA was extracted using RNA-Bee-RNA Isolation Reagent (Tel-Test Inc.). Then, 1 μg of total RNA was reverse-transcribed using Omniscript RT (Qiagen) according to the manufacturer's protocol. Quantitative RT–PCR was performed with TaqMan technology using the ABI Prism 7000 detection system (Applied Biosystems) according to the manufacturer's instructions. RT–PCR conditions were 2 min at 50°C, 10 min at 95°C, and 40 cycles of 15 s at 95°C and 1 min at 60°C. Data were normalized to 18S ribosome or GAPDH level. Each sample was analyzed in duplicate and the experiments were replicated twice for the full set of genes. For 18S ribosome, GAPDH, VEGFR1, and VEGFR2, primers and probes were obtained using TaqMan Assays-on-Demand gene expression products (Applied Biosystems). For NRP1, primer sequences were as follows: sense 5′-CAAGGTGTTCATGAGGAAGTTCAA, antisense 5′-CCGCAGCTCAGGTGTATCATAGT, probe FAM-5′-TGACAGCAAACG CAAGGCGAAGTCTT-TAMRA.

Co-immunoprecipitation assay

HEK293T cells in a 60 mm dish were transfected with 5 μg of pEF-DEST51/VEGFR2 V5 using Lipofectamine 2000. Two days after transfection, we treated the cells with both 10 mU heparitinase and 200 mU chondroitinase in serum-free medium to eliminate extracellular GAG for 2 h at 37°C. Then, cells were lysed in lysis buffer (1% Nonidet P-40, 0.15 M NaCl, 20 mM Tris pH 7.2, including protease inhibitor cocktail (Nacalai)). We also prepared four sets of endogenous CASMCs (100 mm plate, each), which were treated with heparitinase alone, chondroitinase alone, both heparitinase and chondroitinase, or none in serum-free medium for 2 h at 37°C. We then mixed with the aliquot of enzyme-treated VEGFR2 V5 cell lysates and the lysate of each enzyme-treated CASMCs and incubated with anti-V5 agarose (Sigma) in the presence or absence of VEGF (50 ng/ml) for 3 h at 4°C. After extensive washing, immunoprecipitated samples were subjected to SDS–PAGE and Western blotting.

Pulse–chase experiments

HUVECs were transfected with control or N-G siRNA. Two days after transfection, cells were labeled for 20 min at 37°C with 20 μCi [^{35}S]methionine per milliliter in methionine-free Dulbecco's modified Eagle's medium (DMEM; Invitrogen). The cells were then washed and chased in DMEM containing 10% FBS for the indicated time periods. At each time point of the chase, cell lysates were immunoprecipitated with anti-VEGFR2 antibody (C-1158) for 2 h at 4°C. The immunoprecipitates were subjected to SDS–PAGE using 5% polyacrylamide gel. Labeled VEGFR2 was visualized by autoradiography and quantified using the BAS system (Fuji).

Generation of stable cell line

We generated 293 cells which stably expressed VEGFR2 using the Flp-In system (Invitrogen) according to manufacturer's instructions. After VEGFR2 cDNA in the pENTR/D-TOPO was recombined to pEF5/FRT/V5-DEST (Invitrogen), we transfected this construct to Flp293 cells (Invitrogen) with Lipofectamine 2000 (Invitrogen) and established the 293/VEGFR2 cells by selection with 250 μg/ml hygromycin (Invitrogen).

Immunofluorescent staining

Flp293/VEGFR2 cells were transfected with pDEST51-NRP1 FLAG using Optifect (Invitrogen) on a poly-D-lysine-coated chamber-slide (Nunc). Two days later, cells were fixed with 2% paraformaldehyde in PBS for 15 min at room temperature, washed twice in 0.1 M glycine/PBS, and blocked with 10% FBS/PBS for 30 min at room temperature. The cells were probed with anti-VEGFR2 antibody (1:400 dilution in 10% FBS/PBS) for 1 h, then washed and incubated with AlexaFluor 488-conjugated goat antibody against mouse IgG (1:1000 dilution in 10% FBS/PBS; Molecular Probes) for 1 h. The cells were washed thoroughly and then probed with anti-FLAG M2 antibodies conjugated with Cy3 (1:1000 dilution in 10% FBS/PBS; Sigma) for 1 h. We mounted the preparations using

PermaFluor Mountant Medium (Thermo) and took images with Radiance 2100 (Bio-Rad).

Data analysis

Statistical significance was assessed with ANOVA using the Fisher's *post hoc* test. A value of $P<0.05$ was considered to be statistically significant.

Supplementary data

Supplementary data are available at *The EMBO Journal* Online.

Acknowledgements

We thank Drs M Takahashi, N Taniguchi, S Yamada, and H Kitagawa for thoughtful discussion, and A Ogal, Y Nagamachi, H Okuda, and M Nakamura for technical assistance. We thank Drs T Toyofuku and R Iwamoto for reading the manuscript. This study is supported by Grant-in-aid for Scientific Research (nos.16390225, 17390229) from the Ministry of Education, Science and Culture, Japan, a Grant from Japan Cardiovascular Research Foundation, and the Human Frontier Science Program.

References

Bachelder RE, Lipscomb EA, Lin X, Wendt MA, Chadborn NH, Eickholt BJ, Mercurio AM (2003) Competing autocrine pathways involving alternative neuropilin-1 ligands regulate chemotaxis of carcinoma cells. *Cancer Res* **63:** 5230–5233

Benjamin LE, Hemo I, Keshet E (1998) A plasticity window for blood vessel remodelling is defined by pericyte coverage of the preformed endothelial network and is regulated by PDGF-B and VEGF. *Development* **125:** 1591–1598

Blaauwgeers HG, Holtkamp GM, Rutten H, Witmer AN, Koolwijk P, Partanen TA, Alitalo K, Kroon ME, Kijlstra A, van Hinsbergh VW, Schlingemann RO (1999) Polarized vascular endothelial growth factor secretion by human retinal pigment epithelium and localization of vascular endothelial growth factor receptors on the inner choriocapillaris. Evidence for a trophic paracrine relation. *Am J Pathol* **155:** 421–428

Carmeliet P (2003) Angiogenesis in health and disease. *Nat Med* **9:** 653–660

Carmeliet P, Ng YS, Nuyens D, Theilmeier G, Brusselmans K, Cornelissen I, Ehler E, Kakkar VV, Stalmans I, Mattot V, Perriard JC, Dewerchin M, Flameng W, Nagy A, Lupu F, Moons L, Collen D, D'Amore PA, Shima DT (1999) Impaired myocardial angiogenesis and ischemic cardiomyopathy in mice lacking the vascular endothelial growth factor isoforms VEGF164 and VEGF188. *Nat Med* **5:** 495–502

Duval M, Bedard-Goulet S, Delisle C, Gratton JP (2003) Vascular endothelial growth factor-dependent down-regulation of Flk-1/KDR involves Cbl-mediated ubiquitination. Consequences on nitric oxide production from endothelial cells. *J Biol Chem* **278:** 20091–20097

Elbashir SM, Harborth J, Lendeckel W, Yalcin A, Weber K, Tuschl T (2001) Duplexes of 21-nucleotide RNAs mediate RNA interference in cultured mammalian cells. *Nature* **411:** 494–498

Esko JD, Zhang L (1996) Influence of core protein sequence on glycosaminoglycan assembly. *Curr Opin Struct Biol* **6:** 663–670

Ferrara N, Gerber HP, LeCouter J (2003) The biology of VEGF and its receptors. *Nat Med* **9:** 669–676

Fuh G, Garcia KC, de Vos AM (2000) The interaction of neuropilin-1 with vascular endothelial growth factor and its receptor flt-1. *J Biol Chem* **275:** 26690–26695

Gallagher JT (2001) Heparan sulfate: growth control with a restricted sequence menu. *J Clin Invest* **108:** 357–361

Gerber HP, Dixit V, Ferrara N (1998) Vascular endothelial growth factor induces expression of the antiapoptotic proteins Bcl-2 and A1 in vascular endothelial cells. *J Biol Chem* **273:** 13313–13316

Gitay-Goren H, Soker S, Vlodavsky I, Neufeld G (1992) The binding of vascular endothelial growth factor to its receptors is dependent on cell surface-associated heparin-like molecules. *J Biol Chem* **267:** 6093–6098

Grosskreutz CL, Anand-Apte B, Duplaa C, Quinn TP, Terman BI, Zetter B, D'Amore PA (1999) Vascular endothelial growth factor-induced migration of vascular smooth muscle cells *in vitro*. *Microvasc Res* **58:** 128–136

Gu C, Rodriguez ER, Reimert DV, Shu T, Fritzsch B, Richards LJ, Kolodkin AL, Ginty DD (2003) Neuropilin-1 conveys semaphorin and VEGF signaling during neural and cardiovascular development. *Dev Cell* **5:** 45–57

Hurwitz H, Fehrenbacher L, Novotny W, Cartwright T, Hainsworth J, Heim W, Berlin J, Baron A, Griffing S, Holmgren E, Ferrara N, Fyfe G, Rogers B, Ross R, Kabbinavar F (2004) Bevacizumab plus irinotecan, fluorouracil, and leucovorin for metastatic colorectal cancer. *N Engl J Med* **350:** 2335–2342

Ishida A, Murray J, Saito Y, Kanthou C, Benzakour O, Shibuya M, Wijelath ES (2001) Expression of vascular endothelial growth factor receptors in smooth muscle cells. *J Cell Physiol* **188:** 359–368

Jain RK (2003) Molecular regulation of vessel maturation. *Nat Med* **9:** 685–693

Kantor DB, Chivatakarn O, Peer KL, Oster SF, Inatani M, Hansen MJ, Flanagan JG, Yamaguchi Y, Sretavan DW, Giger RJ, Kolodkin AL (2004) Semaphorin 5A is a bifunctional axon guidance cue regulated by heparan and chondroitin sulfate proteoglycans. *Neuron* **44:** 961–975

Kawasaki T, Kitsukawa T, Bekku Y, Matsuda Y, Sanbo M, Yagi T, Fujisawa H (1999) A requirement for neuropilin-1 in embryonic vessel formation. *Development* **126:** 4895–4902

Khurana R, Zhuang Z, Bhardwaj S, Murakami M, De Muinck E, Yla-Herttuala S, Ferrara N, Martin JF, Zachary I, Simons M (2004) Angiogenesis-dependent and independent phases of intimal hyperplasia. *Circulation* **110:** 2436–2443

Kitsukawa T, Shimono A, Kawakami A, Kondoh H, Fujisawa H (1995) Overexpression of a membrane protein, neuropilin, in chimeric mice causes anomalies in the cardiovascular system, nervous system and limbs. *Development* **121:** 4309–4318

Kolodkin AL, Levengood DV, Rowe EG, Tai YT, Giger RJ, Ginty DD (1997) Neuropilin is a semaphorin III receptor. *Cell* **90:** 753–762

Loconto J, Papes F, Chang E, Stowers L, Jones EP, Takada T, Kumanovics A, Fischer Lindahl K, Dulac C (2003) Functional expression of murine V2R pheromone receptors involves selective association with the M10 and M1 families of MHC class Ib molecules. *Cell* **112:** 607–618

Mamluk R, Gechtman Z, Kutcher ME, Gasiunas N, Gallagher J, Klagsbrun M (2002) Neuropilin-1 binds vascular endothelial growth factor 165, placenta growth factor-2, and heparin via its b1b2 domain. *J Biol Chem* **277:** 24818–24825

McLatchie LM, Fraser NJ, Main MJ, Wise A, Brown J, Thompson N, Solari R, Lee MG, Foord SM (1998) RAMPs regulate the transport and ligand specificity of the calcitonin-receptor-like receptor. *Nature* **393:** 333–339

Rubin C, Gur G, Yarden Y (2005) Negative regulation of receptor tyrosine kinases: unexpected links to c-Cbl and receptor ubiquitylation. *Cell Res* **15:** 66–71

Saint-Geniez M, D'Amore PA (2004) Development and pathology of the hyaloid, choroidal and retinal vasculature. *Int J Dev Biol* **48:** 1045–1058

Saito H, Kubota M, Roberts RW, Chi Q, Matsunami H (2004) RTP family members induce functional expression of mammalian odorant receptors. *Cell* **119:** 679–691

Shalaby F, Rossant J, Yamaguchi TP, Gertsenstein M, Wu XF, Breitman ML, Schuh AC (1995) Failure of blood-island formation and vasculogenesis in Flk-1-deficient mice. *Nature* **376:** 62–66

Soker S, Miao HQ, Nomi M, Takashima S, Klagsbrun M (2002) VEGF165 mediates formation of complexes containing VEGFR-2 and neuropilin-1 that enhance VEGF165-receptor binding. *J Cell Biochem* **85:** 357–368

Soker S, Takashima S, Miao HQ, Neufeld G, Klagsbrun M (1998) Neuropilin-1 is expressed by endothelial and tumor cells as an isoform-specific receptor for vascular endothelial growth factor. *Cell* **92:** 735–745

Stalmans I, Lambrechts D, De Smet F, Jansen S, Wang J, Maity S, Kneer P, von der Ohe M, Swillen A, Maes C, Gewillig M, Molin DG, Hellings P, Boetel T, Haardt M, Compernolle V, Dewerchin M, Plaisance S, Vlietinck R, Emanuel B, Gittenberger-de Groot AC,

Scambler P, Morrow B, Driscol DA, Moons L, Esguerra CV, Carmeliet G, Behn-Krappa A, Devriendt K, Collen D, Conway SJ, Carmeliet P (2003) VEGF: a modifier of the del22q11 (DiGeorge) syndrome? *Nat Med* **9:** 173–182

Takashima S, Kitakaze M, Asakura M, Asanuma H, Sanada S, Tashiro F, Niwa H, Miyazaki Ji J, Hirota S, Kitamura Y, Kitsukawa T, Fujisawa H, Klagsbrun M, Hori M (2002) Targeting of both mouse neuropilin-1 and neuropilin-2 genes severely impairs developmental yolk sac and embryonic angiogenesis. *Proc Natl Acad Sci USA* **99:** 3657–3662

Veikkola T, Alitalo K (1999) VEGFs, receptors and angiogenesis. *Semin Cancer Biol* **9:** 211–220

West DC, Rees CG, Duchesne L, Patey SJ, Terry CJ, Turnbull JE, Delehedde M, Heegaard CW, Allain F, Vanpouille C, Ron D, Fernig DG (2005) Interactions of multiple heparin binding growth factors with neuropilin-1 and potentiation of the activity of fibroblast growth factor-2. *J Biol Chem* **280:** 13457–13464

Zachary I (2001) Signaling mechanisms mediating vascular protective actions of vascular endothelial growth factor. *Am J Physiol Cell Physiol* **280:** C1375–C1386

Basic Res Cardiol 101:465–470 (2006)
DOI 10.1007/s00395-006-0603-6

Hideaki Kanzaki
Satoshi Nakatani
Naoaki Yamada
Shin-ichi Urayama
Kunio Miyatake
Masafumi Kitakaze

Impaired systolic torsion in dilated cardiomyopathy: Reversal of apical rotation at mid-systole characterized with magnetic resonance tagging method

Received: 2 November 2005
Returned for revision: 22 November 2005
Revision received: 20 April 2006
Accepted: 11 May 2006
Published online: 16 June 2006

Presented in part at the Annual Scientific Session of ACC 2004 in New Orleans, USA
There are no financial obligations that could lead to conflict of interest regarding this study.

H. Kanzaki, MD · S. Nakatani, MD · K. Miyatake, MD · M. Kitakaze, MD
Department of Cardiology
National Cardiovascular Center
Osaka, Japan

S. Nakatani, MD (✉)
Department of Cardiology
National Cardiovascular Center
5-7-1, Fujishiro-dai, Suita
Osaka 565-8565, Japan
Tel.: +81-6/6833-5012
Fax: +81-6/6872-7486
E-Mail: nakatas@hsp.ncvc.go.jp

N. Yamada, MD
Department of Radiology
National Cardiovascular Center
Osaka, Japan

S.-I. Urayama, PhD
Department of Investigative Radiology
National Cardiovascular Center Research Institute
Osaka, Japan

Abstract Left ventricular (LV) torsion plays an important role in squeezing the blood out of the heart. To characterize the systolic torsion in LV dysfunction, we studied using magnetic resonance imaging myocardial tagging method in 26 subjects: 17 patients with dilated cardiomyopathy (DCM, LV ejection fraction [EF], 27 ± 8 %) and 9 healthy control subjects. Grid-tagged LV short-axis cine images were acquired at base, mid and apex levels. Tag-intersections were tracked during the systole, thereby determining rotation angle (positive indicated clockwise from the apex). Peak torsion was defined as the maximum difference in rotation angle between the base and apex. Time to peak torsion was expressed as % systole by dividing the time by a total systolic time. Amplitude of the rotation at peak was less in DCM than in controls at both the base (0.1 ± 2.9 vs. 2.6 ± 1.6°, $P < 0.05$) and apex (−5.9 ± 5.3 vs. −11.2 ± 2.5°, $P < 0.01$). Amplitude of peak torsion was then less in DCM than in controls (6.1 ± 3.4 vs. 13.6 ± 2.5°, $P < 0.001$), and the timing of peak was earlier (66 ± 22 vs. 104 ± 16 % systole, $P < 0.001$). The amplitude of peak torsion was correlated with LVEF ($r = 0.74$, $P < 0.001$). In conclusion, amplitude of systolic torsion was impaired in proportion to LV function. Systolic torsion in LV dysfunction was characterized by the discontinuing counter-rotation of the apex to the base before end-systole.

Key words magnetic resonance imaging – cardiomyopathy – heart failure – torsion

Abbreviations and Acronyms DCM: dilated cardiomyopathy; ECG: electrocardiogram; LV: left ventricular; LVEDP: LV end-diastolic pressure; LVEDV: LV end-diastolic volume; LVEF: LV ejection fraction; LVESV: LV end-systolic volume; MR: magnetic resonance; NYHA: New York Heart Association; SPAMM: spatial modulation of magnetization

Introduction

The myocardial fibers of the left ventricle vary in orientation across the wall [13, 22, 25]. Greenbaum et al. [13] reported the changes in orientation of the myocardial fibers from a right hand helix in the subendocardium as viewed from the apex, through circumferential fibers in the midwall, to a left hand helix in the subepicardium. Torrent-Guasp et al. [25, 26] have shown that the myocardial fibers constitute a continuous muscular band. The band is oriented spatially as a helix formed by basal and apical loops. Buckberg et al. [4–6] have suggested that the spiral form of myocardial fibers results from twist of the primitive heart evolving from a singular tube. Coghlan et al. [7] proposed that the myocardial

fiber orientation also affects the sequence of activation because of the anisotropic left ventricular (LV) conduction.

During systole, the LV apex rotates in a counterclockwise direction relative to the LV base which rotates in a clockwise direction about LV long-axis as viewed from the apex [30]. This wringing motion is relevant to the shortening of these obliquely oriented LV fibers [21]. Several studies have suggested that LV torsion was sensitive to changes in contractility, but essentially unaffected by changes in pressure or volume loading [3, 15, 17]. However, details of cardiac torsion in patients with impaired LV function still remain unclear.

Several modalities have been used to describe and quantify cardiac torsion, including the magnetic resonance (MR) tagging method with spatial modulation of magnetization (SPAMM). This method makes it possible to label the myocardium non-invasively with spatially selective radiofrequency pulses [1]. Deformation of the tagged pattern reflects the motion of the underlying myocardium to allow tracking the rotation of a LV short-axis plane [2, 19, 29]. Our objective was to characterize LV torsional deformation in patients with impaired LV function using the myocardial MR tagging method.

Methods

Subjects

The study population consisted of a total of 26 subjects. Seventeen patients (15 males, 2 females, age 43 ± 13 years) diagnosed with non-ischemic dilated cardiomyopathy (DCM) from cardiac catheterization were enrolled (Table 1). There was no subject with left bundle branch block (LBBB) on electrocardiogram (ECG). Both LV volumes and EF were measured from left ventriculogram.

Table 1 Characteristics of 17 patients with dilated cardiomyopathy

NYHA functional class, *n* (%)	
I	13 (76)
III	3 (18)
IV	1 (6)
LVEDV, ml	145 ± 65
LVESV, ml	110 ± 65
LVEF, %	27 ± 8
LVEDP, mmHg	12 ± 5
Cardiac index, L/min/m^2	3.4 ± 0.8
Heart rate, beats/min	73 ± 15
QRS duration, ms	105 ± 12

Data are expressed number (%) or mean ± SD
DCM dilated cardiomyopathy; *NYHA* New York Heart Association, *LVEDV* LV end-diastolic volume; *LVESV* LV end-systolic volume; *LVEF* LV ejection fraction; *LVEDP* LV end-diastolic pressure

The diagnosis of DCM was made from the definitions of the World Health Organization. Nine healthy volunteers performed only MR imaging as controls (9 males, age 34 ± 6 years). All provided written informed consent. The study was approved by the ethics committee and performed according to institutional ethics guidelines.

MR image acquisition

MR imaging was performed on a Magnetom Vision 1.5T system (Siemens Medical Solutions, Erlangen, Germany). First of all, the LV long-axis view was obtained to determine three short-axis planes: the basal (chordae tendineae), mid (papillary muscles), and apical planes (Fig. 1). Secondly as shown in Fig. 2, grids with 8-mm spacing were impressed on the myocardium in the LV short-axis view using the spatial modulation of magnetization (SPAMM) method after the R-wave from ECG. The MR tagged cine images were acquired with a breath-hold segmented k-space sequence. Imaging parameters were as follows: image reconstruction interval, 35 ms; 7 segments echo time, 4 ms; flip angle, 20°; the field of view, 350 × 350 mm; image matrix size, 256 × 256 pixels; slice thickness, 8 mm.

MR image analysis

The MR images were analyzed off-line on a workstation (Indigo2, Silicon Graphics Inc, Mountain View, CA) with the dedicated software as previously described [27]. In brief, throughout a series of the images, this software can identify and track the grid pattern with distribution of tag intersections to superimpose a meshwork consisting of nodes connected with straight lines (Fig. 2). The nodes within the LV cavity and outside the LV myocardium were removed manually. First of all, the mesh-

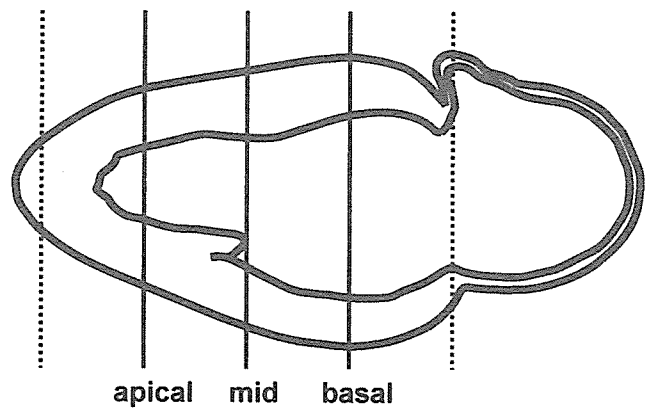

Fig. 1 By dividing equally long-axis of the left ventricle into four compartments, MR tagged short-axis images were acquired at the three levels: chordae tendineae (base), papillary muscles (mid), and apical planes (apex)

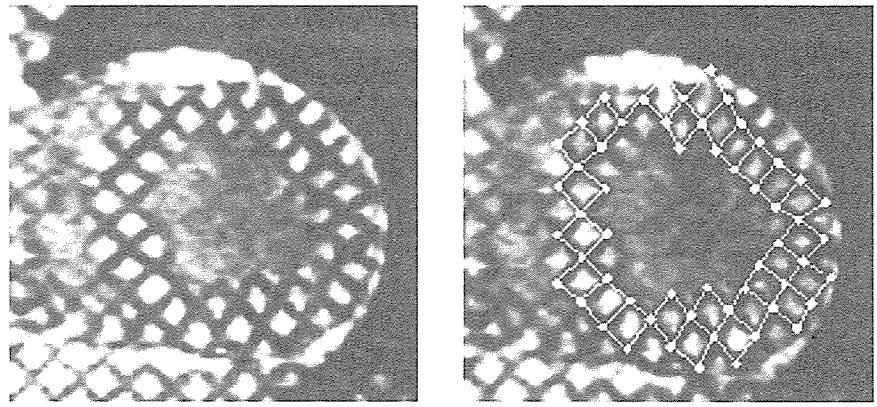

Fig. 2 An acquired image of the mid left ventricular short-axis at end-systole with MR tagging method (Left). A meshwork superimposed on the grid-tag pattern (Right)

work was deformed semi-automatically and then re-formed manually at each image. Finally, the software provided all coordinates of the nodes during systole [27].

Displacement of each node from an initial position was determined during systole as angular displacement relative to the moving centroid at each frame. Rotation angle of each LV short-axis plane was given by averaging measurements from angular displacement of all intersections on the myocardium. LV torsion was defined as the difference in rotation angle between the basal and apical planes (Fig. 3). The gradient of LV torsion was calculated by dividing magnitude of the LV torsion by the distance between the basal and apical planes. Positive degrees indicated a clockwise rotation as viewed from the apex.

We defined the time to peak rotation in % systole as the time from R-wave of ECG to the maximum rotational displacement divided by a total systolic time. LV short-axis diameter was obtained from the inner tag-intersections on the myocardium at the mid LV plane. The total systolic time was measured as the interval from the R-wave to the moment of minimum short-axis diameter of the left ventricle.

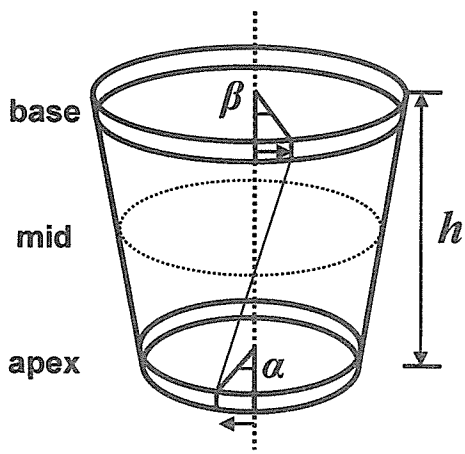

Fig. 3 LV torsion was defined as the difference in rotational angles of basal (β) and apical (α) planes. Torsional gradient was calculated by dividing the LV torsional angle by the distance between the two planes (*h*)

Statistics

Results are expressed as mean values ± SD. Continuous variables were compared with one-way ANOVA. Linear regression analysis was used to assess the relationship between two groups. All statistical tests were performed with StatView 5.0 for Windows (SAS Institute, Cary, USA). Statistical significance was assumed for $P < 0.05$.

Results

Cardiac torsion

In controls (Fig. 4a), both the LV base and apex initially rotated counterclockwise. After 21 ± 6 % systole, the base changed the direction of rotation to clockwise, whereas the apex maintained counter-clockwise rotation until around the end-systole. Peak cardiac torsion of 13.6 ± 2.5° was generated at 104 ± 10 % systole. In other words, the peak of torsion almost coincided with end-systole.

In patients with DCM (Fig. 4b), both base and apex initially rotated counter-clockwise as well. However, the base changed the direction somewhat late (at 27 ± 8 % systole, $P < 0.05$ vs. control), and the apex also followed to turn toward clockwise at mid-systole (at 54 ± 18 % systole, $P < 0.05$ vs. control). Then cardiac torsion peaked at 66 ± 8 % systole in patients with DCM (about 12 % systole behind the apical peak), which was earlier than in controls ($P < 0.001$). The magnitude of torsion in patients with DCM was also markedly impaired (6.1 ± 3.4°, $P < 0.0001$ vs. control).

As shown in Fig. 5, the peak apical rotation in controls was −11.2 ± 2.5° and the basal rotation was 2.6 ± 1.6°, thereby developing the peak LV torsional gra-

Basic Research in Cardiology, Vol. 101, No. 6 (2006)

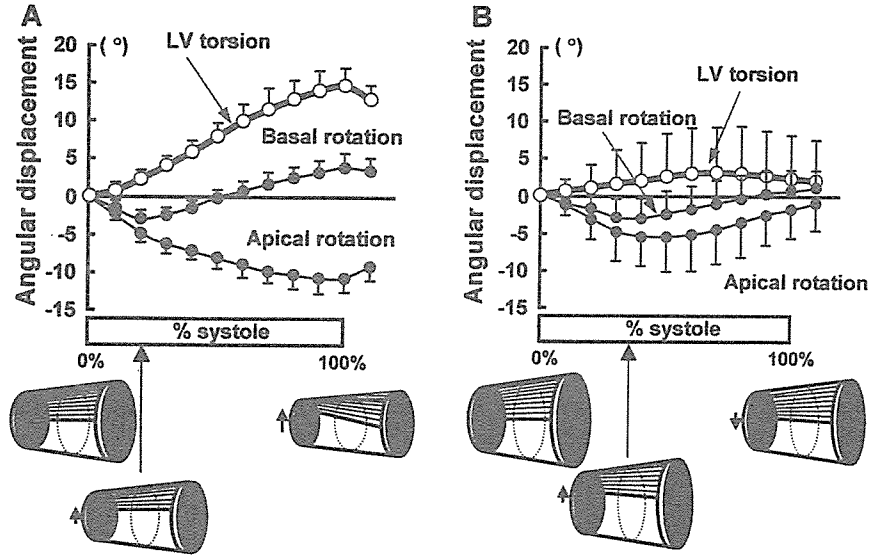

Fig. 4 Time course of LV torsion in controls (**a**) and DCM (**b**): Instantaneous LV torsion (○) was developed from the net difference between the basal and apical rotations (●). Positive degrees indicate a clockwise rotation as viewed from the apex

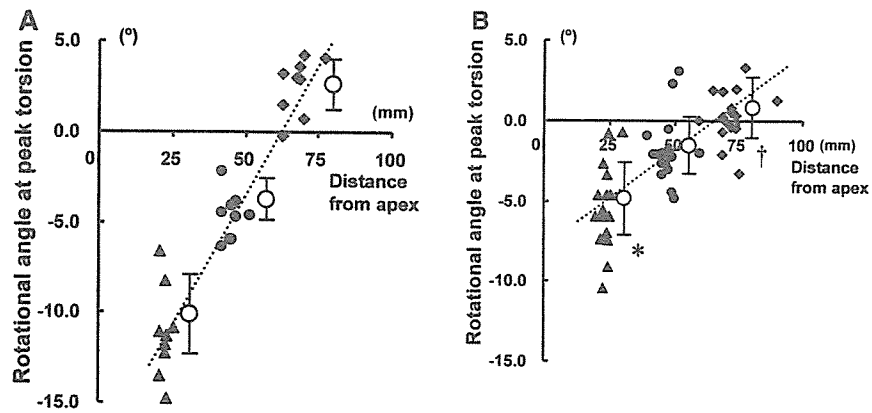

Fig. 5 The rotational angles (of ▲ apical, ● mid, and ◆ basal planes) and the distance from the LV apex at the peak torsion in controls (**a**) and DCM (**b**). The broken line represents the mean of the individual torsional gradients, which was significantly less in DCM than controls. * $P < 0.01$ and ** $P < 0.05$ vs. control. Positive degrees indicate a clockwise rotation as viewed from the apex

dient of 3.0 ± 0.5°/cm. In patients with DCM, the rotation was impaired at the both apical (-5.9 ± 5.3°, $P < 0.01$ vs. control) and basal levels (0.1 ± 2.9°, $P < 0.05$ vs. control). Consequently, the peak LV torsional gradient was markedly impaired (1.3 ± 0.8°/cm, $P < 0.01$ vs. control).

Cardiac torsion and LV function

The magnitude of peak torsion and torsional gradient showed significant correlations with LVEF ($r = 0.74$ and $r = 0.78$, respectively, both $P < 0.001$) as shown in Fig. 6. Time to the peak LV torsion was correlated with the LV end-diastolic volume ($r = -0.71$, $P < 0.005$), end-systolic volume ($r = -0.80$, $P < 0.001$), and magnitude of peak torsion ($r = 0.81$, $P < 0.0001$).

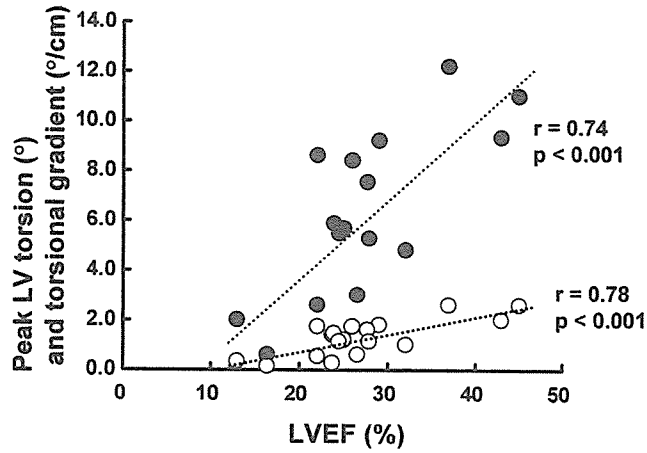

Fig. 6 Peak LV torsional angle (●) and torsional gradient (○) were correlated well with LVEF in patients with DCM

Discussion

The present study revealed that phasic analysis of both apical and basal rotations need to obtain the cardiac torsion of the failing heart. In DCM hearts, at both the basal and apical planes, the amplitude of peak rotation was significantly less than those in normal hearts. The timing of peak torsion did not coincide with the timing of peak apical rotation and the end-systole.

Impaired cardiac torsion in LV dysfunction

The normal control data in Fig. 5 are consistent with the data reported by the group of Hess [18]. The magnitude of peak LV torsion has been reported to be 11–19°, and torsional gradient was 2.8–3.4°/cm in normal humans [2, 14–18, 23, 29]. The present results, $13.6 \pm 2.5°$ and $3.0 \pm 0.5°$/cm, respectively, in controls are consistent with the previous reports, supporting the validity of the present method.

In contrast, the magnitude of peak torsion and torsional gradient in DCM remarkably decreased to $6.1 \pm 3.4°$ and $1.3 \pm 0.8°$/cm, respectively. The peak of torsion was at neither end-systole nor the timing of peak apical rotation, approximately 12% systole behind the apical peak (Fig. 4b). Taber et al. [24] proposed that LV contractility and cavity volume can influence the torsion using theoretical models. LV torsion is due to the decreasing ventricular radius and increasing wall thickness, which further increase the mechanical advantage of the outer layers. In markedly dilated heart, the advantage over the inner layers is lost.

Sallin et al. [22] demonstrated the rationale that the spiral configuration enabled the myocardial fibers with only 15% shortening to generate LVEF up to >60%. Buckberg et al. [5] proposed that flattening of the apical loop architecture in the spheric DCM heart cause reduced LVEF. LV dilatation can make the apical loop become more basal through more transverse fiber orientation.

Significance of LV torsion

Many investigators have focused on cardiac torsion as a sensitive marker of global LV function [12, 14–16, 18–20]. Nagel et al. [18], using the similar grid technique, reported that systolic torsion was correlated with percentage change in LV area determined as regional EF. Dong et al. [8] reported that torsion was correlated with stroke volume and LVEF in animal experiments. We showed the good correlation between the rotational amplitude and LVEF in humans as well (Fig. 6). Rademakers et al. [20] proposed that torsion recoil in diastole could aid LV filling with sucking in blood from the left atrium. Rothfeld et al. [21] demonstrated that LV systolic torsion related with acceleration and acceleration time of mitral early-diastolic filling wave from echocardiography. In other words, cardiac torsion is a possible mechanism by which potential energy can be stored in systole and then released in early diastole to create LV suction [28]. A tight coupling has been reported between contraction and relaxation [9]. Our results showing that cardiac torsion was associated with systolic function may support the idea that cardiac torsion plays a role of a flywheel or pendulum.

Clinical implications

Cardiac resynchronization therapy using a biventricular pacing system is effective for synchronization of wall motion in heart failure patients with LBBB. Recognition of the influences of LBBB on rotation and time-to-peak rotation may help improved understanding of the electrical activation sequence in obliquely oriented myocardial fibers. Fonseca et al. [11] reported that the three dimensional MR tissue tagging technique was useful for analysis on asynchrony and torsion. Recent development of tissue tracking technique of ultrasound also allows easy assessment of torsion in patients with LBBB. Further work in this area is expected.

Study limitations

There are some limitations in the present study. First, use of the tag spacing of 8 mm on the LV myocardium with wall thickness of < 11 mm can lead heterogeneous distribution of the intersecting points [27]. We averaged all values measured from intramyocardial grid-crossing points to assess a rotation of the plane. Reproducibility was not examined. Second, the systolic through-plane motion of short-axis images can cause some error. However, because this motion is remarkable at the base of the left ventricle which shows further less rotation than the apex, the error may not be critical for the present results. Fischer et al. [10] have resolved this problem by tracking the tags on the same slice of the myocardium. Third, frame rate is approximately 30 fps in the MR imaging method. This may be slightly low in measuring the peak value of LV torsion and time to peak torsion. Fourth, the mean age of our control group is less than that of the DCM group. This could be a limitation because of the effect of age. Fifth, no MR imaging data on LV volume was available in the present study. Therefore, we had to use the volume data from left ventriculogram instead of that.

Conclusion

The apex and base rotated with an opposite direction to generate effective torsion at end-systole in normal hearts. In DCM hearts, amplitude of peak LV systolic torsion was impaired in proportion to the global LV function. Systolic torsion in LV dysfunction was characterized by the discontinuing counter-rotation of the apex to the base before end-systole as it might follow the basal motion.

Acknowledgement The authors gratefully acknowledge Mr. Jason Catizone for the preparation of this manuscript and Toshiharu Sakuma, BS RT for the technical assistance.

References

1. Axel L, Dougherty L (1989) MR imaging of motion with spatial modulation of magnetization. Radiology 171:841–845
2. Buchalter MB, Weiss JL, Rogers WJ, Zerhouni EA, Weisfeldt ML, Beyar R, Shapiro EP (1990) Noninvasive quantification of left ventricular rotational deformation in normal humans using magnetic resonance imaging myocardial tagging. Circulation 81:1236–1244
3. Buchalter MB, Rademakers FE, Weiss JL, Rogers WJ, Weisfeldt ML, Shapiro EP (1994) Rotational deformation of the canine left ventricle measured by magnetic resonance tagging: effects of catecholamines, ischaemia, and pacing. Cardiovasc Res 28:629–635
4. Buckberg GD (2001) The structure and function of the helical heart and its buttress wrapping. II. Interface between unfolded myocardial band and evolution of primitive heart. Semin Thorac Cardiovasc Surg 13:320–332
5. Buckberg GD, Coghlan HC, Torrent-Guasp F (2001) The structure and function of the helical heart and its buttress wrapping. VI. Geometric concepts of heart failure and use for structural correction. Semin Thorac Cardiovasc Surg 13:386–401
6. Buckberg GD (2002) Basic science review: the helix and the heart. J Thorac Cardiovasc Surg 124:863–883
7. Coghlan HC, Coghlan AR, Buckberg GD, Gharib M, Cox JL (2001) The structure and function of the helical heart and its buttress wrapping. III. The electric spiral of the heart: The hypothesis of the anisotropic conducting matrix. Semin Thorac Cardiovasc Surg 13: 333–341
8. Dong SJ, Hees PS, Huang WM, Buffer SA Jr, Weiss JL, Shapiro EP (1999) Independent effects of preload, afterload, and contractility on left ventricular torsion. Am J Physiol 277(3 Pt 2):H1053–H1060
9. Eichhorn EJ, Willard JE, Alvarez L, Kim AS, Glamann DB, Risser RC, Grayburn PA (1992) Are contraction and relaxation coupled in patients with and without congestive heart failure? Circulation 85:2132–2139
10. Fischer SE, McKinnon GC, Scheidegger MB, Prins W, Meier D, Boesiger P (1994) True myocardial motion tracking. Magn Reson Med 31:401–413
11. Fonseca CG, Oxenham HC, Cowan BR, Occleshaw CJ, Young AA (2003) Aging alters patterns of regional nonuniformity in LV strain relaxation: a 3-D MR tissue tagging study. Am J Physiol Heart Circ Physiol 285:H621–H630
12. Gibbons Kroeker CA, Tyberg JV, Beyar R (1995) Effects of load manipulations, heart rate, and contractility on left ventricular apical rotation. An experimental study in anesthetized dogs. Circulation 92:130–141
13. Greenbaum RA, Ho SY, Gibson DG, Becker AE, Anderson RH (1981) Left ventricular fibre architecture in man. Br Heart J 45:248–263
14. Hansen DE, Daughters GT 2nd, Alderman EL, Ingels NB Jr, Miller DC (1988) Torsional deformation of the left ventricular midwall in human hearts with intramyocardial markers: regional heterogeneity and sensitivity to the inotropic effects of abrupt rate changes. Circ Res 62:941–952
15. Hansen DE, Daughters GT 2nd, Alderman EL, Ingels NB, Stinson EB, Miller DC (1991) Effect of volume loading, pressure loading, and inotropic stimulation on left ventricular torsion in humans. Circulation 83:1315–1326
16. Ingels NB Jr, Hansen DE, Daughters GT 2nd, Stinson EB, Alderman EL, Miller DC (1989) Relation between longitudinal, circumferential, and oblique shortening and torsional deformation in the left ventricle of the transplanted human heart. Circ Res 64:915–927
17. Moon MR, Ingels NB Jr, Daughters GT 2nd, Stinson EB, Hansen DE, Miller DC (1994) Alterations in left ventricular twist mechanics with inotropic stimulation and volume loading in human subjects. Circulation 89:142–150
18. Nagel E, Stuber M, Lakatos M, Scheidegger MB, Boesiger P, Hess OM (2000) Cardiac rotation and relaxation after anterolateral myocardial infarction. Coron Artery Dis 11:261–267
19. Nakatani S, White RD, Powell KA, Lever HM, Thomas JD (1996) Dynamic magnetic resonance imaging assessment of the effect of ventricular wall curvature on regional function in hypertrophic cardiomyopathy. Am J Cardiol 77: 618–622
20. Rademakers FE, Buchalter MB, Rogers WJ, Zerhouni EA, Weisfeldt ML, Weiss JL, Shapiro EP (1992) Dissociation between left ventricular untwisting and filling. Accentuation by catecholamines. Circulation 85:1572–1581
21. Rothfeld JM, LeWinter MM, Tischler MD (1998) Left ventricular systolic torsion and early diastolic filling by echocardiography in normal humans. Am J Cardiol 81:1465–1469
22. Sallin EA (1969) Fiber orientation and ejection fraction in the human left ventricle. Biophys J 9:954–964
23. Stuber M, Scheidegger MB, Fischer SE, Nagel E, Steinemann F, Hess OM, Boesiger P (1999) Alterations in the local myocardial motion pattern in patients suffering from pressure overload due to aortic stenosis. Circulation 100:361–368
24. Taber LA, Yang M, Podszus WW (1996) Mechanics of ventricular torsion. J Biomech 29:745–752
25. Torrent-Guasp F, Ballester M, Buckberg GD, Carreras F, Flotats A, Carrio I, Ferreira A, Samuels LE, Narula J (2001) Spatial orientation of the ventricular muscle band: physiologic contribution and surgical implications. J Thorac Cardiovasc Surg 122:389–392
26. Torrent-Guasp F, Kocica MJ, Corno AF, Komeda M, Carreras-Costa F, Flotats A, Cosin-Aguillar J, Wen H (2005) Towards new understanding of the heart structure and function. Eur J Cardiothorac Surg 27:191–201
27. Urayama S, Matsuda T, Sugimoto N, Mizuta S, Yamada N, Uyama C (2000) Detailed motion analysis of the left ventricular myocardium using an MR tagging method with a dense grid. Magn Reson Med 44:73–82
28. Waldman LK, Nosan D, Villarreal F, Covell JW (1988) Relation between transmural deformation and local myofiber direction in canine left ventricle. Circ Res 63:550–562
29. Young AA, Imai H, Chang CN, Axel L (1994) Two-dimensional left ventricular deformation during systole using magnetic resonance imaging with spatial modulation of magnetization. Circulation 89:740–752
30. Yun KL, Miller DC (1995) Torsional deformation of the left ventricle. J Heart Valve Dis 4(Suppl 2):S214–S220

J Pharmacol Sci **101**, 179 – 181 (2006)

Journal of Pharmacological Sciences

Correspondence

New Therapeutic Application of Erythropoietin Against Ischemic Heart Diseases

Tetsuo Minamino[1] and Masafumi Kitakaze[2,*]

[1]*Cardiovascular Medicine, Osaka University Graduate School of Medicine, Suita, Osaka 565-0871, Japan*
[2]*Cardiovascular Division of Internal Medicine, National Cardiovascular Center, 5-7-1 Fujishirodai, Suita, Osaka 565-8565, Japan*

Received April 25, 2006

Keywords: myocardial infarction, angiogenesis, ventricular remodeling

Erythropoietin (EPO) is a cytokine that promotes proliferation and differentiation of erythroid precursor cells, and it is widely used for the treatment of anemia in patients with chronic renal failure (1). Therefore, EPO has been classified as one of the hemtopoietic cytokines independent of cardiovascular physiological and biochemical actions. However, intriguingly, EPO can also exert anti-apoptotic and radical scavenging effects on non-erythroid cells (1). Furthermore, EPO receptors are found in cardiovascular systems including endothelial cells and cardiomyocytes (2). These findings suggest that EPO is expected to have some function in cardiovascular systems. Indeed, several investigators showed that an administration of EPO before or shortly after the onset of ischemia reduced myocardial infarct size and improved cardiac function in acute phases (3, 4). Another interesting non-erythroid function of EPO is the promotion of endothelial progenitor cell (EPC) mobilization in animals and humans, which may enhance neovascularization of ischemic areas (5, 6). Recently, Hirata et al. demonstrated that EPO increased EPC and enhances angiogenesis in ischemic myocardium after myocardial infarction (MI) and simultaneously improved cardiac function (7).

Along with these lines of evidence, Nishiya et al. importantly investigated effects of EPO on cardiac remodeling after MI in rats (8). They administered EPO in two different ways: Subcutaneous injection once a day for 4 days at 5,000 U/kg or 3 times a week for 4 weeks at 1,000 U/kg. They found that EPO improved both hemodynamic parameters and cardiac function after MI in both experimental groups. They also found that EPO prevented caspase-3 activation, up-regulation of remodeling-related genes, and the increase in interstitial fibrosis in non-infarcted myocardium. Finally, they showed enhanced angiogenesis and reduced apoptosis in the peri-infarcted myocardium. Their findings provide additional important evidence that EPO exerts cardioprotective effects after ischemia/reperfusion injury. However, if EPO is to be used in clinical applications, there are several important considerations.

Therapeutic dose and time-window

Nishiya et al. demonstrated that the administration of EPO (1,000 – 5,000 U/kg) improved cardiac function after a complete occlusion model of MI (8). The doses of EPO administered were nearly 10 times higher than those clinically used in anemic patients with chronic renal failure (1). Hirata et al. demonstrated that EPO dose-dependently (100 – 1000 IU/kg) reduced infarct size in a canine model of ischemia/reperfusion (7). Further investigation will be needed to determine the optimal dose of EPO for exerting caridoprotective effects in clinical use.

The timing for EPO administration is another important issue that must be solved to apply this agent in clinical practice. Nishiya et al. administered EPO in two different ways: Subcutaneous injection once a day for 4 days or 3 times a week for 4 weeks (8). Several investigators showed that an administration of EPO before or shortly after the onset of ischemia reduced myocardial infarct size and improved cardiac function in acute phases (3, 4). Interestingly, van der Meer et al. demonstrated that EPO started three weeks after MI increased capillary density and simultaneously improved cardiac function in rats with MI (9). Further investigations will be also needed to determine the optimal timing

*Corresponding author. kitakaze@zf6.so-net.ne.jp
Published online in J-STAGE: June 15, 2006
doi: 10.1254/jphs.LTJ06001X

and dose when EPO is applied in clinical practice.

Potential mechanisms by which EPO induces cardioprotection

Reduction of apoptotic cell death

Consistent with previous studies (3, 4), Nishiya et al. demonstrated that EPO decreased the number of TUNEL-positive cells in the peri-infarcted myocardium, suggesting that EPO prevents apoptotic cell death (8). However, since the TUNEL method also detects single strand breaks occurring in the course of necrotic cell death, it is likely that EPO attenuates apoptotic and necrotic cell death. Indeed, if EPO only inhibits the apoptotic cell death, it may be difficult to explain the marked reduction of infarct size by EPO. Recent reports suggest that EPO can inhibit the release of free radicals from neutrophils and act as a radical scavenger (1), both of which may reduce cardiac cell death after ischemia/reperfusion and attenuate cardiac remodeling.

Angiogenesis

Nishiya et al. showed enhanced angiogenesis in the peri-infarcted myocardium, which may contribute to the improvement of cardiac function after MI (8). Consistent with their report, we also found that EPO increased the number of EPC and angiogenesis in the ischemic myocardium (7). Interestingly, Nishiya et al. demonstrated that long-term administration of EPO significantly increased vessel density compared to short-term administration of EPO. Although EPO is a powerful stimulator of EPC mobilization from the bone marrow, it also has pro-angiogenetic effects (10). These different angiogenetic effects of EPO might explain the result of Nishiya's study.

Prevention of remodeling in the non-infarcted areas

Recent studies have highlighted the importance of fibrosis of non-infarcted areas remote from the site of infarction for the pathogenesis of post-infarction cardiac dysfunction (11, 12). Nishiya et al. clearly demonstrated that EPO prevented caspase-3 activation, up-regulation of remodeling-related genes, and the increase in interstitial fibrosis in non-infarcted myocardium. Prevention of cardiac remodeling in the non-infarcted myocardium will also contribute to the EPO-induced improvement of cardiac function after MI.

Clinical relevance

Recently, a higher endogenous EPO level can predict a smaller infarct size in patients with acute MI subjected to successful primary percutaneous coronary intervention (13). These findings support the idea that an administration of EPO would exert cardioprotective effects against acute ischemia reperfusion injury and cardiac remodeling. However, we must be careful of thromboembolism when we apply EPO in the clinical situation. A high dose (40,000 – 60,000 IU per week) of subcutaneously administered EPO increased the incidence of thrombotic events such a venous thrombosis or pulmonary embolisms in patients with breast cancer (14). On the other hand, in a previous clinical study, a high dose (33,000 IU once daily for the first 3 days) of intravenously administered EPO was well tolerated in patients with stroke and improved clinical outcome at 1 month (15). Careful clinical study will be warranted if EPO is to be applied for the treatment of patients with acute MI.

Although considerable future work will be required, EPO is a potentially promising candidate for an adjunctive therapy for acute MI and cardiac remodeling, and Nishiya et al. largely and importantly contributed to the paradigm of EPO in the field of cardiovascular protection.

References

1 Fisher JW. Erythropoietin: physiology and pharmacology update. Exp Biol Med (Maywood). 2003;228:1–14.
2 Wright GL, Hanlon P, Amin K, Steenbergen C, Murphy E, Arcasoy MO. Erythropoietin receptor expression in adult rat cardiomyocytes is associated with an acute cardioprotective effect for recombinant erythropoietin during ischemia-reperfusion injury. FASEB J. 2004;18:1031–1033.
3 Hirata A, Minamino T, Asanuma H, Sanada S, Fujita M, Tsukamoto O, et al. Erythropoietin just before reperfusion reduces both lethal arrhythmias and infarct size via the phosphatidylinositol-3 kinase-dependent pathway in canine hearts. Cardiovasc Drugs Ther. 2005;19:33–40.
4 Calvillo L, Latini R, Kajstura J, Leri A, Anversa P, Ghezzi P, et al. Recombinant human erythropoietin protects the myocardium from ischemia reperfusion injury and promotes beneficial remodeling. Proc Natl Acad Sci U S A. 2003;100:4802–4806.
5 Heeschen C, Aicher A, Lehmann R, Fichtlscherer S, Vasa M, Urbich C, et al. Erythropoietin is a potent physiologic stimulus for endothelial progenitor cell mobilization. Blood. 2003;102:1340–1346.
6 Bahlmann FH, DeGroot K, Duckert T, Niemczyk E, Bahlmann E, Boehm SM, et al. Endothelial progenitor cell proliferation and differentiation is regulated by erythropoietin. Kidney Int. 2003;64:1648–1652.
7 Hirata A, Minamino T, Asanuma H, Sanada S, Fujita M, Wakeno M, et al. Erythropoietin enhances neovascularization of ischemic myocardium and improves left ventricular dysfunction after myocardial infarction in dogs. Circulation. 2005;112:II–199.
8 Nishiya D, Omura T, Shimada K, Matsumoto R, Kusuyama T, Enomoto S, et al. Effects of erythropoietin on cardiac remodel-